学位論文（要約）

Development of Novel Synthesis Methods for Carbon-Nitrogen Based Two-Dimensional Crystals

（炭素-窒素系二次元結晶の新規成長手法の開発）

平成 29 年 12 月　博士（理学）申請

東京大学大学院理学系研究科

化学専攻

加藤　時穂

ABSTRACT

Two-dimensional (2D) crystals, materials with a thickness of only one or a few atoms thick, has been drawing more and more attention to their wide range of potential applications. Among 2D crystals, nitrogen-doped graphene (N-Gr) and graphitic carbon nitride (g-C_3N_4) are exceptionally attractive with its potential for next-generation electronics and energy storage devices. These 2D crystals are also known as cost-effective and eco-friendly materials because these are composed of common and abundant elements of carbon and nitrogen atoms. Though fabrication methods of these 2D crystals are yet to be developed, there is a currently huge gap between the expectations and reality. A key requirement for application of 2D crystals is the development of synthesis method. In this thesis, two novel synthesis methods are developed for two different carbon-nitrogen based 2D crystals.

In chapter 1, an overview of 2D crystals, including properties, applications, synthesis, and characterization was introduced. Then motivation and scope of this thesis were presented.

In chapter 2, to achieve the site-selective synthesis of N-Gr, a novel chemical vapor deposition (CVD) method was devised. The N-Gr synthesis was focused on controlling the configurations of three doping sites in graphene lattice: graphitic-N, pyridinic-N, and pyrrolic-N site. In the method, six kinds of N-containing heterocyclic compounds were selected as a source molecule and deposited on a heated Pt (111). The N-Gr with pyridinic-N and pyrrolic-N were exclusively obtained from quinoline and pyrrole molecules at 500 °C, and N-Gr with graphitic-N was synthesized from methyl-form at 400 °C. As a consequence, three doping sites were successfully controlled by using the structure of molecular precursors.

In chapter 3, the synthesis of 2D g-C_3N_4 was examined by using the same CVD method as the chapter 2. In the method, melamine was chosen as a source molecule and deposited on Pt (111) and Cu (111) at different temperatures. On Pt (111) substrate, melamine was

already decomposed at room temperature, indicates strong catalytic activity of the substrate. On the other hand, a self-assembled 2D network of melamine was observed for the first time on Cu (111) at 400 °C and graphene were formed at 500 °C. Even though the g-C_3N_4 was not formed, valuable findings were obtained from the results.

In chapter 4, based on these results and ideas from chapter 3, a novel fabrication method using solid/solid interface was presented and conducted to synthesize 2D g-C_3N_4. The chapter included the process of developing the novel synthesis method begins with the concept of interfacial polymerization and continues throughout the entire design of solid/solid interfacial synthesis of 2D g-C_3N_4. In the method, melamine sandwiched between two solids: a sapphire substrate and Au thin-film were annealed and polymerized to form g-C_3N_4. As a result, thin-film of g-C_3N_4 with the thickness of around 1 nm was obtained. Therefore, the formation of 2D g-C_3N_4 was confirmed.

In chapter 5, an overall conclusion of this thesis was stated. In this thesis, two 2D crystals composed of carbon and nitrogen: N-Gr and 2D g-C_3N_4 were synthesized by novel methods. The N-Gr synthesis was focused on controlling the configurations of three doping sites, and fabrication of 2D g-C_3N_4 was concentrated on creating a large-area crystalline monolayer structure. Finally, significance and prospect of this study were represented.

CONTENTS

CHAPTER 1

Introduction to Two-Dimensional Crystals

1.1 Properties and applications of 2D crystals

1.1.1 Graphene

Two-dimensional crystals, materials with a thickness of only one or a few atoms thick, have been drawing more and more attention for their wide range of potential applications since 2004. In this year, a single atomic layer of carbon atoms called graphene, also known as the first two-dimensional crystal, was experimentally demonstrated by mechanical exfoliation of graphite.[1] Graphene consists of sp^2 carbon atoms bonding in a hexagonal lattice as shown in Figure 1.1. Graphene has attracted many scientists with its extraordinary properties such as high carrier mobility,[2] high thermal conductivity,[3] high surface area,[4,5] and high Young's modulus.[6] The electronic application is one of the most promising application fields for graphene. With its ultrahigh carrier mobility of 200,000 cm^2/Vs, which is 200 times faster than that of silicon, graphene is desired for a channel

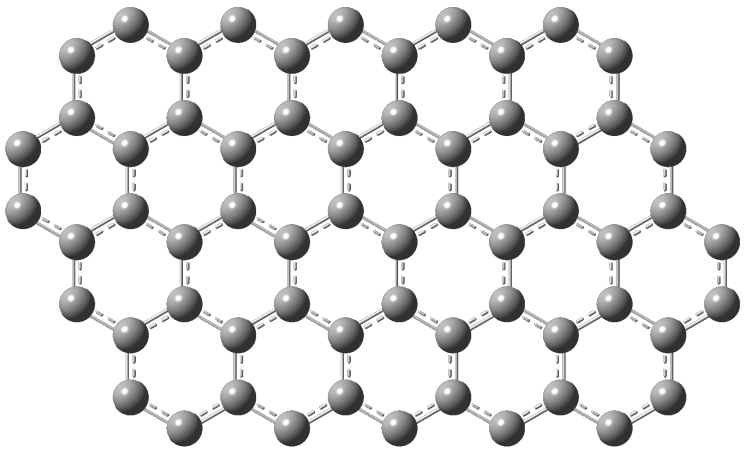

Figure 1.1 Schematic illustration of the structure of graphene

material for field effect transistors (FET). However, the lack of bandgap limits its application in electronic devices (Fig. 1.2).

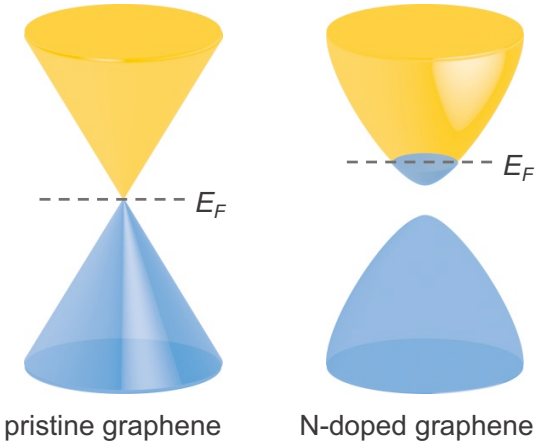

Figure 1.2 Energy band Structure of graphene and N-Gr

1.1.2 Nitrogen-doped graphene (N-Gr)

The electrical properties of graphene can be modulated by doping of heteroatoms like boron,[7,8] or nitrogen.[9,10] Many theoretical and experimental studies proved that B or N doped graphene gains band gap efficiently and behaves as p or n-type semiconductors.[11,12] Substitutional doping of hexagonal carbon lattice with heteroatoms enables graphene to modulate the electronic, chemical or structural properties. Among a variety of such heteroatoms, nitrogen is a hopeful candidate for modifying properties of graphene due to its comparable atomic size and providing an additional valence electron. Figure 1.3 shows schematic illustrations of the structure of the nitrogen-doped graphene (N-Gr). N-Gr has attracted much attention due to their potential for electronic applications such as field effect transistor, lithium ion batteries[13] and ultracapacitors.[14] Further, N-Gr is also expected as a metal-free catalyst for oxygen reduction reaction for its fascinating catalytic potential.[15,16] Thus, the nitrogen functionalization of graphene is a promising way to bring further fascinating properties to graphene and open the door to its various applications. These electronic or catalytic properties of nitrogen-doped graphene (N-Gr) are significantly affected by the doping site of the nitrogen atom (Figure 1.3). Three common bonding configurations: graphitic-, pyridinic-, and pyrrolic-N embedded within the

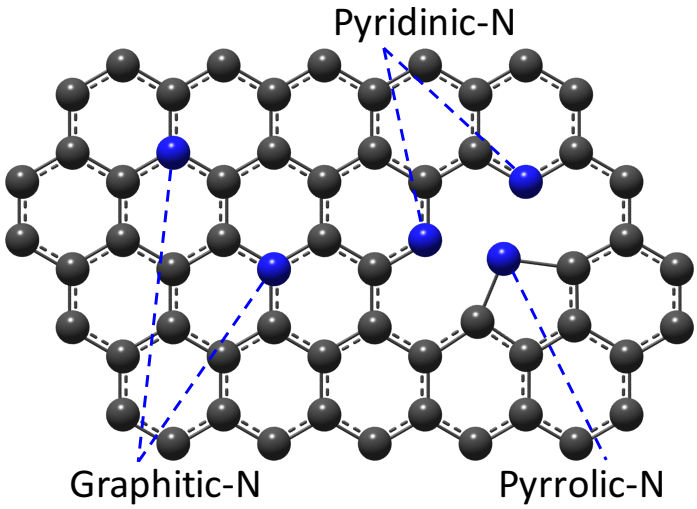

Figure 1.3 Schematic illustration of the chemical structure of N-Gr

carbon lattice, play essential roles in determining the properties. N-type doping occurs for graphitic-N whereas p-type doping takes place at pyridinic- and pyrrolic-N. Modifying electronic states by such N-doping opens the band gap and enhances the catalytic activity of oxygen reduction reaction while non-doped graphene has no band gap (Figure 1.2). Therefore, controlling the doping site is crucial for tuning or tailoring the properties of N-Gr. Figure 1.4 shows the schematic illustration of N-Gr containing 2.1 atomic % of

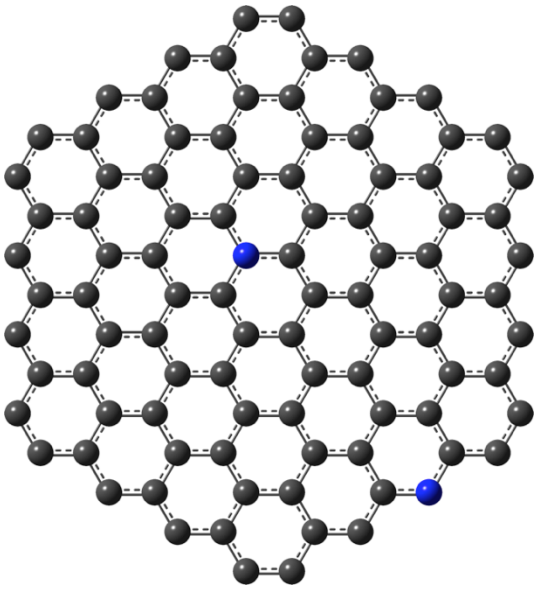

Figure 1.4 Schematic illustration of N-Gr containing 2.1 atomic % of nitrogen. The graphene is formed by 94 carbon atoms and 2 nitrogen atoms which are doped at graphitic-, and pyridinic-N sites.

nitrogen.

1.1.3 Two-dimensional graphitic carbon nitride (2D g-C_3N_4)

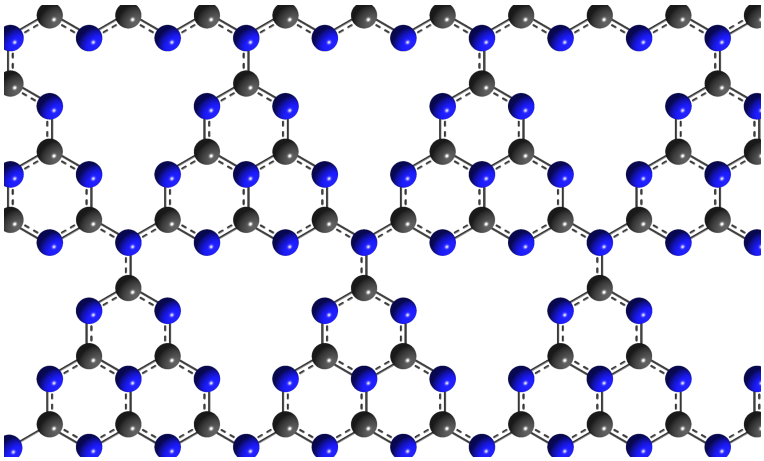

Figure 1.5 Chemical structure of g-C_3N_4 (heptazine based polymer melon)

2D graphitic carbon nitride (g-C_3N_4): crystalline 2D conjugated polymer an analogy to graphene is a 2D material made of "ubiquitous" carbon and nitrogen atoms. Figure 1.5 shows the structure of 2D g-C_3N_4. The heptazine based polymer melon as known as g-C_3N_4 is composed of the periodic arrangement of the condensed melem (tri-s-triazine) units.[17,18] The structure of g-C_3N_4 is similar to graphite. They both have stacked layers bonded with only van der Waals interlayer interaction and strong covalent bonds of C-N for g-C_3N_4, and C-C for graphite in each layer. Carbon nitride (melon) is also known as one of the oldest synthetic polymers prepared from in 1834 by Liebig from the pyrolysis of melamine ($C_3H_6N_6$).[19] Since then, a lot of fascinating properties of carbon nitride was reported. For example, the presence of the β-C_3N_4 which is a superhard material predicted to be harder than diamond was first proposed in 1985.[20,21]

Nowadays, g-C_3N_4 have attracted much attention for its potential applications in visible-light driven semiconductor photocatalysts due to its unique electrical,[22,23] optical,[24–26] and photocatalytic properties.[27–31] The bulk material of g-C_3N_4 has an intrinsic bandgap of 2.7 eV which is suitable for visible light and has the ability for photocatalytic water splitting,[25,29] Diels-Alder reactions,[28] and Friedel-Crafts reactions.[31] The catalytic activity

increased as the thickness of g-C_3N_4 gets decreased because of the increased specific surface area. Therefore, 2D g-C_3N_4 is expected as the promising candidate for the new generation photocatalyst with metal-free, low-cost, outstanding visible-light-driven photocatalyst.

1.2 Synthesis method of 2D crystals

The synthesis methods of 2D crystals can be divided into following two types of approaches: top-down and bottom-up method. As the name implies, the top-down method prepares 2D crystal via its bulk or initial material. The initial material is processed to the 2D crystal in the method. The process is miniaturization in general, such as physical/chemical exfoliation, and photo/electron-beam lithography techniques. The typical top-down synthesis method begins with the bulk material and reduces into nano-scale. The bottom-up method, on the other hand, directly forms 2D crystal from basic units of material (atoms or molecules). During the process, molecules or atoms self-assembly forms the large and stable 2D structure by the assist of physical or chemical forces.

As an example, top-down approach prepares graphene from the exfoliation of HOPG (highly oriented pyrolytic graphite) and bottom-up for chemical vapor deposition (CVD) from methane gas. CVD is a widely used technique to deposit thin films that supply source material as a gas phase to react on the surface. The CVD method is a notable candidate for large area and high-quality production of graphene. Figure 1.6 shows the top-down and the bottom-up approaches of the synthesis of N-Gr. A top-down approach produces N-doped graphene with substituting carbon atoms with nitrogen atoms via post-treatment to graphene (initial material). Nitrogen incorporation via UV-irradiation in ammonia,[32] and nitrogen plasma treatment,[33] for example, have been reported. In a bottom-up approach, on the other hand, nitrogen atoms are incorporated into graphene during the growth process. Same as the graphene, CVD is the most typical and the most promising bottom-up fabrication method for preparing a large-area and high-quality

nitrogen-doped graphene. In this process, nitrogen-doping coincides with graphene formation.

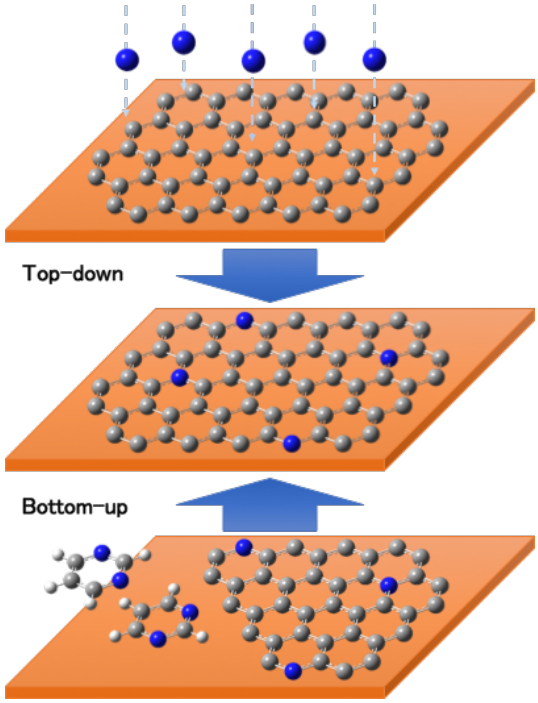

Figure 1.6 Schematic representation of top-down and bottom-up synthesis of N-Gr

1.3 Transfer of 2D crystals

As stated in the former section, CVD is a promising method for large area and high-quality synthesis of 2D crystal. The as-prepared 2D crystal by CVD is bonded to the growth substrate with interactions. For the characterization or the application, 2D crystal requires to be free from the substrate or transferred to another substrate. Thus, the transfer technique of 2D crystals is significantly important. The conventional transfer of 2D crystal is to dissolve the growth substrate. In fact, copper, commonly used as a growth substrate of graphene, was dissolved by dipping into the etchant (nitric acid). In this study, platinum single crystal substrate was mainly used for the CVD substrate, as mentioned in later chapters. Since the growth substrate is extremely expensive, the dissolving method is unrealistic for this study. To transfer the 2D crystal from the growth substrate, a non-destructive transfer method called bubbling transfer method which uses the electrolysis

of water was conducted in this study. Figure 1.7 shows the procedure of the bubbling transfer method.[34] At first, the film of polymethyl methacrylate (PMMA) was fabricated on graphene/Pt substrate. Then PMMA/graphene/Pt was dipped into aqueous NaOH. Then the DC voltage of 3.4 V was supplied with connecting PMMA/graphene/Pt as a cathode and pristine Pt as an anode. H_2 bubble generates at cathode from the following reaction.

$$2H_2O(l) + 2e^- \rightarrow H_2(g) + 2OH^-(aq)$$

After few seconds, graphene with PMMA separates from Pt substrate. After that, PMMA was removed by dipping into acetone.

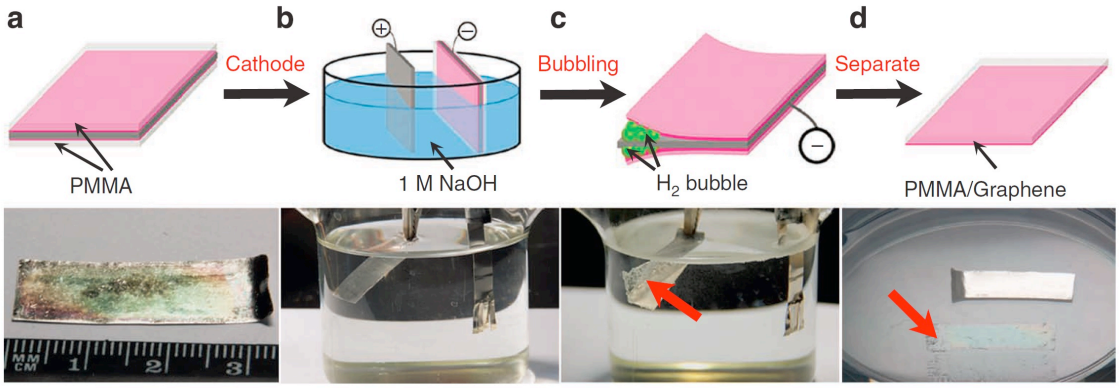

Figure 1.7 Schematic illustration of bubbling transfer method,[34] (Reprinted by permission from Nature Publishing group; Macmillan Publishers Ltd: [Nat. Commun.] (L. Gao *et al*., 2012).

1.4 Characterization techniques of 2D crystals

1.4.1 X-ray photoelectron spectroscopy (XPS)

X-ray photoelectron spectroscopy (XPS), or as known as electron spectroscopy for chemical analysis (ESCA) is a qualitative and quantitative spectroscopic technique that uses soft X-ray sources. The XPS allows measuring both elemental composition and chemical states of a material surface using the following photoelectric effect.

$$E_b = h\nu - E_k - \phi$$

Where E_k is the kinetic energy of photoelectron and hv is the photon energy of X-ray and φ is the work function of the analyzer. The binding energy (E_b) is obtained by measuring the kinetic energy of photoelectron. The kinetic energy of emitted photoelectrons is measured at hemispherical analyzer as shown in Figure 1.8. XPS analyses the average chemical composition by measuring the kinetic energy and counting the number of photoelectrons which are ejected from the outermost surface (depth of 1-10 nm). The measurement must be conducted in ultrahigh vacuum (UHV) environment with the base pressure around 10^{-7} Pa. As stated, there are two types of X-ray sources: Mg Kα radiation (hv = 1253.6 eV) and Al Kα radiation (hv = 1486.6 eV). In this study, Mg Kα radiation (1253.6 eV) (Thermo VG Scientific XR3E2) was used as the X-ray source, and photoelectrons were analyzed by the hemispherical analyzer (SPECS, PHOIBOS-100).

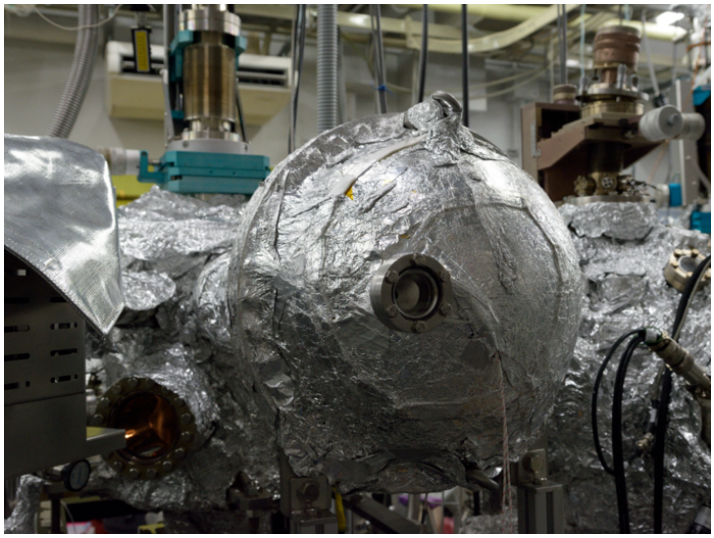

Figure 1.8 Picture of hemispherical analyzer of XPS (SPECS, PHOIBOS-100).

1.4.2 Low energy electron diffraction (LEED)

Low energy electron diffraction (LEED) is a technique that analyses the surface structure of the crystalline material in both qualitatively and quantitatively by using low energy electron beam (20-200 eV). LEED shows the diffraction patterns of backscattered electrons from the surface of the sample on its fluorescent screen as spots. The diffraction

pattern is generated only when the Ewald sphere intersects reciprocal lattice rods (vectors). The LEED pattern shows 2D reciprocal lattice of the sample surface. The LEED pattern enables to evaluate the size, symmetry, and orientation of unit cell of the crystal surface. Same as XPS, LEED is also very sensitive to surface and requires to be conducted in UHV condition. In this thesis, the LEED analysis was performed with a beam energy of 100-200 eV. Figure 1.9 shows the picture of LEED analyzer (OCI BDL800IR-MCP2).

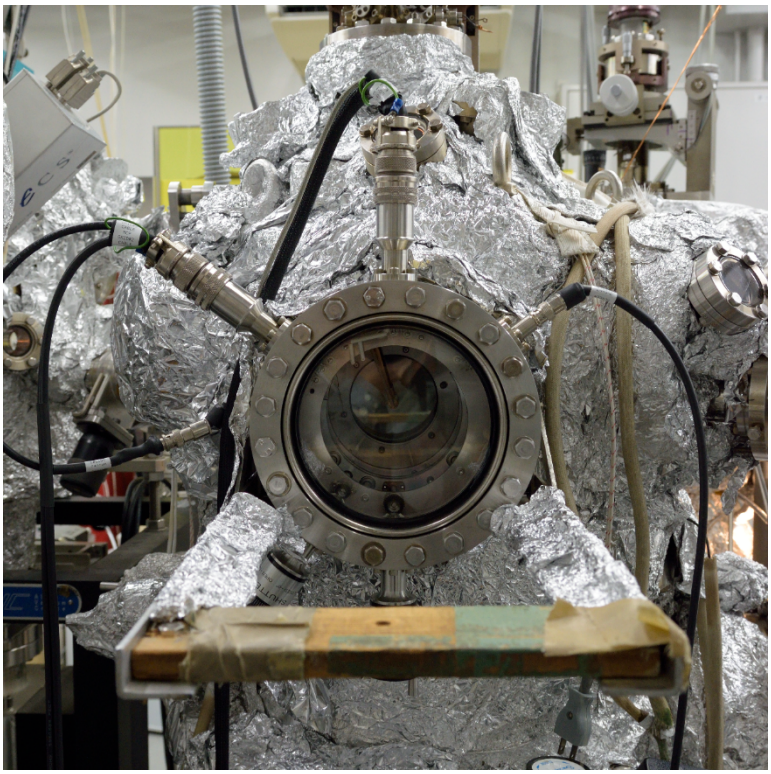

Figure 1.9 Picture of LEED-AES spectrometer (OCI BDL800IR-MCP2)

1.4.3 Raman spectroscopy

Raman spectroscopy is the qualitative spectroscopic technique widely used to assign or evaluate the surface structure by observing the rotational and vibrational movement. It uses the monochromatic laser light to observe Raman scattering (inelastic scattering). Raman scattering is one of the inelastic scattering of photons by phonons or molecular vibrations. The difference in frequency (or energy) between incident light (photons) and

inelastically scattered light (photons) is defined as a Raman shift. The measurement can be operated in Air, and it permits a wide range of materials without preparation. In this study, the Raman measurement was performed with excitation laser wavelength of 532 nm. Figure 1.10 shows the picture of Raman spectrometer (JASCO, NRS-3100).

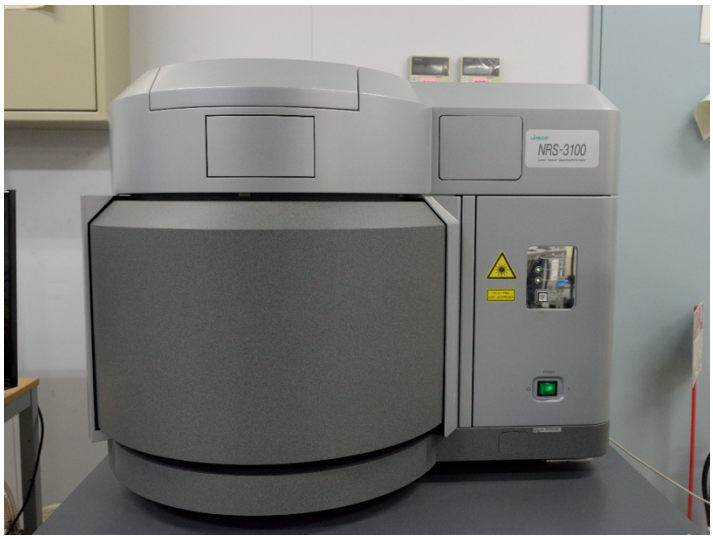

Figure 1.10 Picture of Raman spectrometer (JASCO, NRS-3100)

1.4.4 Atomic force microscopy (AFM)

Atomic force microscopy (AFM) is a sort of scanning probe microscope (SPM) that measures the force between the AFM probe tip which is held at the end of the cantilever and the surface of the sample. AFM was invented in 1985.[36] AFM is quite surface sensitive that it can sense the various forces such as van der Waals, electrostatic, magnetic and capillary forces. Therefore, it requires optimizing measurement conditions like shapes and materials of the AFM probe or measurement atmospheres to measure the demanded particular force. AFM exhibits a very high sensitivity of the height direction. It generates an image of the sample surface by scanning the AFM tip across the surface. AFM is a versatile SPM technique that permits the topographic imaging of conductive or non-conductive surface under air or vacuum conditions. Figure 1.11 shows the AFM setup used in this study. The AFM (JEOL, JSPM-4210) observation was carried out in the air

with the non-contact mode (AC mode).

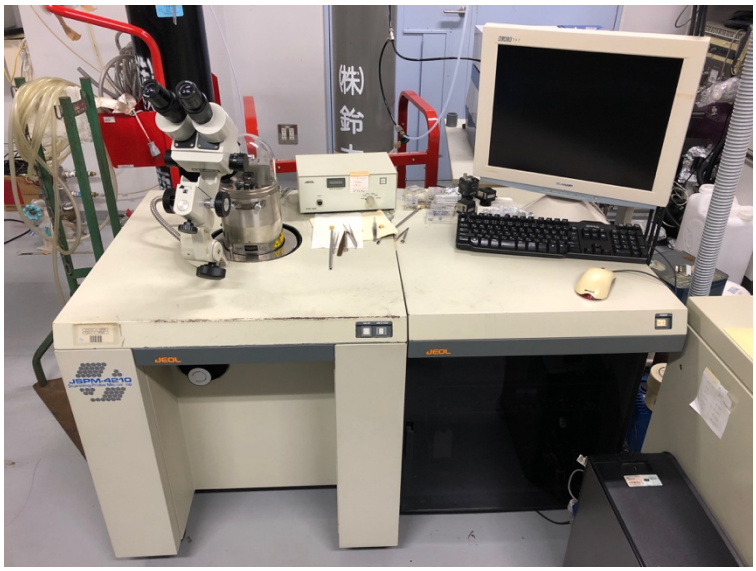

Figure 1.11 Picture of AFM setup (JEOL, JSPM-4210)

1.5 Motivation and scope of this thesis

Recently, 2D crystals are drastically increasing its number. However, fabrication methods are not keeping up with the discovery of 2D crystals. In fact, many kinds of 2D crystals are still fabricated by the mechanical exfoliation (top-down method) of the bulk material because of the lack of bottom-up synthesis method. Further, industrial applications of 2D crystal are limited by the lack of its mass-production method (bottom-up method). The bottom-up synthesis method is also a key requirement for the application of 2D crystals. This study is focused on developing the bottom-up synthesis method of 2D crystals, especially for N-Gr and 2D g-C_3N_4. Among the 2D crystals, these two require the effective bottom-up synthesis method and are exceptionally attractive with its potential for next-generation electronics and energy storage devices. Therefore, this thesis aimed to develop bottom-up synthesis methods for two carbon-nitrogen based 2D crystals.

1.6 References

1. K. S. Novoselov, A. K. Geim, S. V. Morozov, D. Jiang, Y. Zhang, S. V. Dubonos, I. V. Grigorieva and A. A. Firsov, *Science*, 2004, **306**, 666–669.
2. K. I. Bolotin, K. J. Sikes, Z. Jiang, M. Klima, G. Fudenberg, J. Hone, P. Kim and H. L. Stormer, *Solid State Commun.*, 2008, **146**, 351–355.
3. A. A. Balandin, S. Ghosh, W. Bao, I. Calizo, D. Teweldebrhan, F. Miao and C. N. Lau, *Nano Lett.*, 2008, **8**, 902–907.
4. A. Peigney, C. Laurent, E. Flahaut, R. R. Bacsa and A. Rousset, *Carbon N. Y.*, 2001, **39**, 507–514.
5. M. D. Stoller, S. Park, Z. Yanwu, J. An and R. S. Ruoff, *Nano Lett.*, 2008, **8**, 3498–3502.
6. C. Lee, X. Wei, J. W. Kysar and J. Hone, *Science*, 2008, **321**, 385–388.
7. L. S. Panchakarla, K. S. Subrahmanyam, S. K. Saha, A. Govindaraj, H. R. Krishnamurthy, U. V. Waghmare and C. N. R. Rao, *Adv. Mater.*, 2009, **21**, 4726–4730.
8. Z.-H. Sheng, H.-L. Gao, W.-J. Bao, F.-B. Wang and X.-H. Xia, *J. Mater. Chem.*, 2012, **22**, 390–395.
9. D. Wei, Y. Liu, Y. Wang, H. Zhang, L. Huang and G. Yu, *Nano Lett.*, 2009, **9**, 1752–1758.
10. L. Qu, Y. Liu, J.-B. Baek and L. Dai, *ACS Nano*, 2010, **4**, 1321–1326.
11. D. Usachov, O. Vilkov, A. Grüneis, D. Haberer, A. Fedorov, V. K. Adamchuk, A. B. Preobrajenski, P. Dudin, A. Barinov, M. Oehzelt, C. Laubschat and D. V. Vyalikh, *Nano Lett.*, 2011, **11**, 5401–5407.
12. A. Lherbier, A. R. Botello-Méndez and J.-C. Charlier, *Nano Lett.*, 2013, **13**, 1446–1450.

13. Z. S. Wu, W. Ren, L. Xu, F. Li and H. M. Cheng, *ACS Nano*, 2011, **5**, 5463–5471.

14. H. M. Jeong, J. W. Lee, W. H. Shin, Y. J. Choi, H. J. Shin, J. K. Kang and J. W. Choi, *Nano Lett.*, 2011, **11**, 2472–2477.

15. Q. Han, B. Wang, J. Gao, Z. Cheng, Y. Zhao, Z. Zhang and L. Qu, *ACS Nano*, 2016, **10**, 2745–2751.

16. D. Geng, Y. Chen, Y. Chen, Y. Li, R. Li, X. Sun, S. Ye and S. Knights, *Energy Environ. Sci.*, 2011, **4**, 760.

17. S. Chu, C. Wang, J. Feng, Y. Wang and Z. Zou, *Int. J. Hydrogen Energy*, 2014, **39**, 13519–13526.

18. B. Jürgens, E. Irran, J. Senker, P. Kroll, H. Müller and W. Schnick, *J. Am. Chem. Soc.*, 2003, **125**, 10288–10300.

19. H. May, *J. Appl. Chem.*, 1959, **9**, 340–344.

20. M. L. Cohen, *Phys. Rev. B*, 1985, **32**, 7988–7991.

21. A. Y. Liu and M. L. Cohen, *Science*, 1989, **245**, 841–842.

22. G. Algara-Siller, N. Severin, S. Y. Chong, T. Björkman, R. G. Palgrave, A. Laybourn, M. Antonietti, Y. Z. Khimyak, A. V. Krasheninnikov, J. P. Rabe, U. Kaiser, A. I. Cooper, A. Thomas and M. J. Bojdys, *Angew. Chemie - Int. Ed.*, 2014, **53**, 7450–7455.

23. M. M. Dong, C. He and W. X. Zhang, *J. Mater. Chem. C*, 2017, **5**, 3830–3837.

24. Y. Zhang, Q. Pan, G. Chai, M. Liang, G. Dong, Q. Zhang and J. Qiu, *Sci. Rep.*, 2013, **3**, 1943.

25. Y. Yuan, L. Zhang, J. Xing, M. I. B. Utama, X. Lu, K. Du, Y. Li, X. Hu, S. Wang, A. Genç, R. Dunin-Borkowski, J. Arbiol and Q. Xiong, *Nanoscale*, 2015, **7**, 12343–12350.

26. A. Wang, C. Wang, L. Fu, W. Wong-Ng and Y. Lan, *Nano-Micro Lett.*, 2017, **9**, 47.

27. W. J. Ong, L. L. Tan, Y. H. Ng, S. T. Yong and S. P. Chai, *Chem. Rev.*, 2016, **116**, 7159–7329.

28. Y. Zhao and M. Antonietti, *Angew. Chemie - Int. Ed.*, 2017, **56**, 9336–9340.

29. J. Liu, Y. Liu, N. Liu, Y. Han, X. Zhang, H. Huang, Y. Lifshitz, S. T. Lee, J. Zhong and Z. Kang, *Science*, 2015, **347**, 970–974.

30. X. Wang, K. Maeda, A. Thomas, K. Takanabe, G. Xin, J. M. Carlsson, K. Domen and M. Antonietti, *Nat. Mater.*, 2009, **8**, 76–80.

31. F. Goettmann, A. Fischer, M. Antonietti and A. Thomas, *Angew. Chemie Int. Ed.*, 2006, **45**, 4467–4471.

32. G. Imamura and K. Saiki, *Chem. Phys. Lett.*, 2013, **587**, 56–60.

33. K. Akada, T. Terasawa, G. Imamura, S. Obata and K. Saiki, *Appl. Phys. Lett.*, 2014, **104**, 131602.

34. L. Gao, W. Ren, H. Xu, L. Jin, Z. Wang, T. Ma, L. P. Ma, Z. Zhang, Q. Fu, L. M. Peng, X. Bao and H. M. Cheng, *Nat. Commun.*, 2012, **3**, 699.

35. A. Eckmann, A. Felten, A. Mishchenko, L. Britnell, R. Krupke, K. S. Novoselov and C. Casiraghi, *Nano Lett.*, 2012, **12**, 3925–3930.

36. G. Binnig, C. F. Quate and C. Gerber, *Phys. Rev. Lett.*, 1986, **56**, 930–933.

CHAPTER 2

Site-Selective Synthesis of Nitrogen-Doped Graphene from Nitrogen-Containing Heterocyclic Compounds

In this chapter, a novel method is devised to develop and establish a new approach for the site-selective synthesis of nitrogen-doped graphene. As stated in the former chapter, nitrogen heteroatoms are mainly doped at three different sites in graphene lattice: graphitic-N, pyridinic-N, and pyrrolic-N site. The electronic or catalytic properties of nitrogen-doped graphene are significantly affected by these N-doped sites. This means that the controlling the doping site is crucial for tuning or tailoring the properties. Thus, it is highly expected to develop methods to realize a selective formation of nitrogen configurations in graphene networks. In this work, site-selective synthesis of nitrogen-doped graphene was examined using six kinds of nitrogen-containing heterocyclic compounds as sources.

In the first section gives an overview of general backgrounds of structure, properties, applications and synthesis of nitrogen-doped graphene, and the objective of this study is expressed.

The second section describes details on experimental methods of sample preparation and characterization. It also contains the detailed explanations on each of the source molecules. Especially, reasons and motivations for the selections of each molecule are referred here.

The following two sections are devoted to present results and discussions on attempts of preparing pyridinic- and pyrrolic-N doped graphene from nitrogen-containing aromatic compounds and graphitic-N doped graphene from nitrogen-embedded cyclic triarylamines, respectively.

The final section gives conclusions which include the importance and significance of this work.

2.1 Introduction

Graphene is a single layer of graphite which consists of sp^2 carbon atoms arranged in a hexagonal lattice. Since its first isolation in 2004,[1] graphene has attracted scientists by its fascinating properties.[2–5] Doping of graphene with heteroatoms is expected to bring about further intriguing properties of graphene.[6,7] Among a variety of such heteroatoms, nitrogen is a hopeful candidate for modifying properties of graphene due to its comparable atomic size and providing an additional valence electron. First-principles calculations predicted the presence of a band-gap, which would realize large on/off ratio in field effect transistors.[8] Moreover, catalytic activity for oxygen reduction reaction has been reported for nitrogen-doped graphene.[9,10] The most compelling feature of N-doping is that the doped site has a significant effect on the electronic properties of the graphene.[11,12] There are three types of N-doping sites in graphene: graphitic-, pyridinic-, and pyrrolic-N. Both theoretical and experimental studies have proved that graphitic-N causes n-type doping whereas pyridinic- and pyrrolic-N give rise to p-type doping.[12–14] As for applications, pyridinic-N improves the performance of Li-ion battery by enhancing Li-ion intercalation.[14,15] Although many studies have reported the synthesis of N-doped graphene, efficient methods of controlling the amount and site of nitrogen atoms in graphene are yet to be developed.

The synthesis methods of N-doped graphene are divided into two types: top-down and bottom-up approaches.[16,17] A top-down approach produces N-doped graphene with substituting carbon atoms with nitrogen atoms via post-treatment to graphene or graphene oxide.[18,19] Nitrogen incorporation via UV-irradiation in ammonia,[20,21] and nitrogen plasma treatment,[12,22–24] for example, have been reported. In a bottom-up approach, on the other hand, nitrogen atoms are incorporated into graphene during the growth process. Chemical vapor deposition (CVD) is the most typical and the most promising bottom-up fabrication method for preparing a large-area and high-quality nitrogen-doped

graphene.[25] In this process, nitrogen-doping coincides with graphene formation. CVD synthesis of N-doped graphene have been performed mostly on transition metal substrates such as Ni,[26,27] Cu,[28–35] and Pt.[36,37] Especially, platinum is an excellent substrate due to its chemical stability; platinum is not easily oxidized or evaporated compared to other transition metals. Moreover, with that stability, platinum does not require co-flow of hydrogen gas or argon carrier gas during the CVD process. Another advantage of using platinum as a CVD substrate is its rather weak interaction with graphene,[38] and thus the property of the grown graphene is less affected by the substrate. Also, the graphene on the Pt substrate could be transferred to the different substrate with ease and less damage (mentioned in the following section). Platinum forms graphene without help of other gases, which enables to synthesize graphene from a single source molecule.[36–39] Single-source CVD uses a molecule that could have suitable chemical composition and structure. On single-source CVD, it can be expected that N atoms are doped into graphene with preserving and reflecting the structure of source molecules, leading to the control of doped sites. Furthermore, the method has an advantage in observing the relationship between the structure of source molecules and as-synthesized N-doped graphene.Therefore, the single-source CVD is a promising method not only for controlling the structure but also for understanding the growth mechanism.

In this study, nitrogen-doped graphene was synthesized on Pt (111) by the single-source CVD in ultra-high vacuum (UHV) and analyzed *in-situ*. In such well-controlled conditions, the graphene is free from contamination during both synthesis and analysis, which assures the precise evaluation of N-doped site and content. Though the previous study indicated the effect of source molecule on the nitrogen doping,[36] structural control of N-doped graphene is yet to be accomplished, or the mechanism of nitrogen doping via single-molecule CVD is still unclear. The present work conducted single-source CVD using six kinds of nitrogen-containing heterocyclic compounds to achieve the structure control of N-doped graphene. These molecules are used to aim at controlling doping sites with reflecting their N-bonding configurations to graphene. With this approach, site-selective N-doping to graphene at three representative sites: graphitic-N, pyridinic-N, and

pyrrolic-N sites are examined and discussed. Based on the relationship between the structure of as-prepared graphene and the source molecule, the growth mechanisms of nitrogen-doped graphene are also discussed.

2.2 Experimental

2.2.1 Source molecules

As mentioned in the introduction of this chapter, appropriate selection of source molecule is the most crucial factor in the site-selective synthesis of nitrogen-doped graphene. In this study, the configuration of the nitrogen atom in a molecule is expected as the key factor. Three N-doped sites which are graphitic-N, pyridinic-N, and pyrrolic-N site can be distinguished from one another by their nitrogen-bonding configurations. Pyridinic- and pyrrolic-N has two-coordinated nitrogen atom whereas graphitic-N has three-coordinated one. Pyridinic-N has a nitrogen atom at the hexagonal edge, while at the pentagonal edge in pyrrolic-N. By taking the structural characteristics of N-doped sites into account, source molecules which are similar to these doped structures are chosen.

Figure 2.1 shows six compounds, in each of which are chosen as a source molecule:(a) quinolone (C_9H_7N), (b) pyridine (C_5H_5N), (c) pyrrole (C_4H_5N), (d) pyrimidine ($C_4H_4N_2$), (e) 4,4,8,8,12,12-hexamethyl-8,12-dihydro-4H-benzo[9,1]quinolizino[3,4,5,6,7-defg]acridine ($C_{27}H_{27}N$), and (f) 4H-benzo[9,1]quinolizino[3,4,5,6,7-defg]acridine-4,8,12-trione ($C_{21}H_9NO_3$). Pyridine has a nitrogen atom contained in its six-membered benzene ring (Figure 2.1(b)). Meanwhile, pyrimidine has two N-atoms in it (Figure 2.1(d)). Likewise, quinoline also has a nitrogen-atom involved in naphthalene ring (Figure 2.1(a)). All three molecules have one or two two-coordinated nitrogen atom in the linkage, which is expected as an efficient precursor for forming pyridinic-N doped graphene. Preparing the graphenes from different single sources is effective for elucidating the growth mechanisms through the relationship of source molecules and fabricated graphenes. Pyrrole (Figure 2.1(c)) is chosen as its imitating structure to the pyrrolic-N site. These four aromatic compounds: quinoline, pyridine, pyrrole, pyrimidine

are all liquid reagents at room temperature. With comparing Figure 2.1(e) and Figure 2.1(f), there is a little difference in their peripheral structure that bridges the benzene rings. For convenience, the molecule that has three dimethylmethylene bridges is expressed as the methyl-form (Figure 2.1(e)), and the other triketone molecule is referred to as the ketone-form (Figure 2.1(f)) in this thesis. These two compounds are solid reagents and were prepared by following existing protocols.[40,41] In these molecules, each of the nitrogen atom is linked to three carbon atoms via a single bond and is tightly embedded into a graphitic fashion in the molecular framework, which keeps the plane to be flat. The

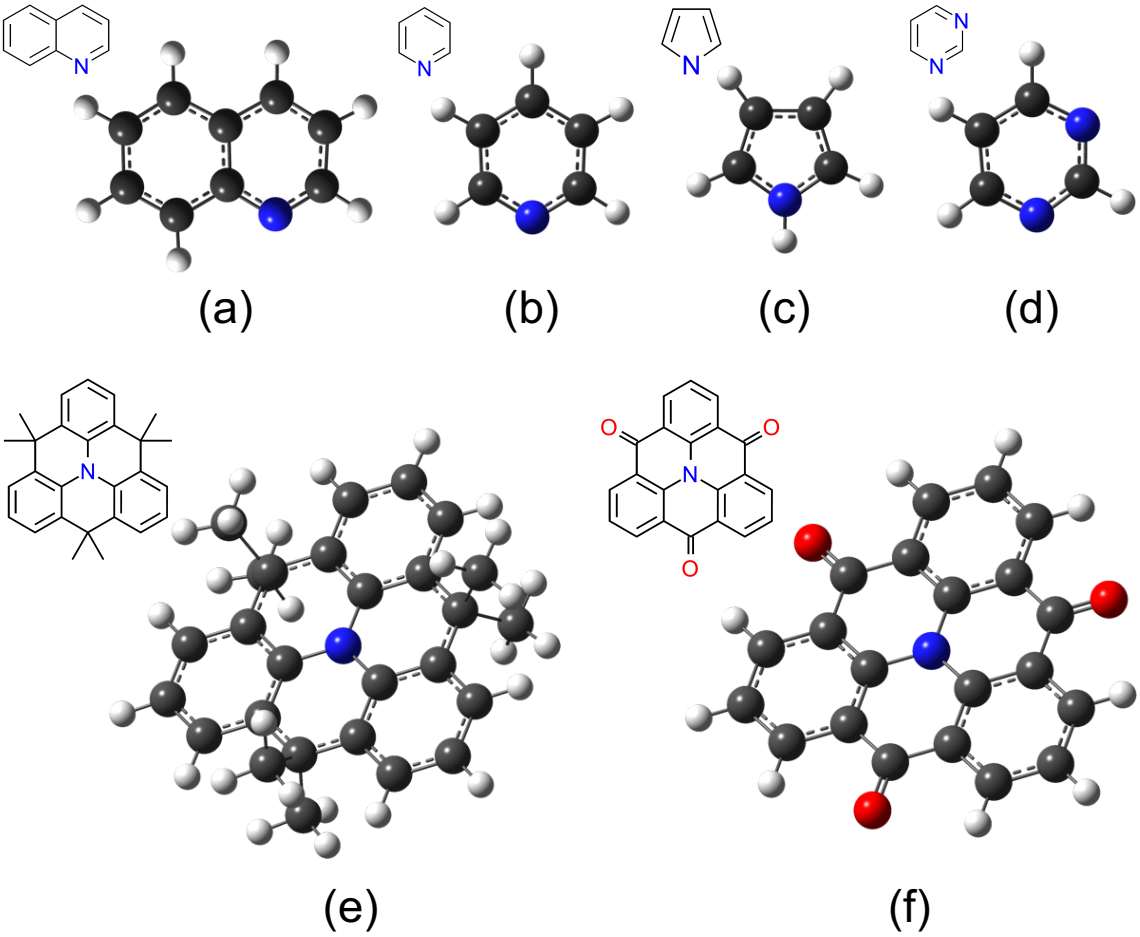

Figure 2.1 Molecular structures of the source molecules (given in 2D and 3D representations): (a) quinolone, (b) pyridine, (c) pyrrole, (d) pyrimidine, (e) 4,4,8,8,12,12-hexamethyl-8,12-dihydro-4H-benzo[9,1]quinolizino[3,4,5,6,7-defg]acridine (methyl-form), and (f) 4H-benzo [9,1]quinolizino[3,4,5,6,7-defg]acridine-4,8,12-trione (ketone-form).

structure of these molecules is predicted as favorable for incorporating nitrogen atoms into the graphitic-N site of the graphene lattice during the CVD process.

2.2.2 Sample synthesis and characterization

Film growth by CVD and the surface analysis were conducted in an ultrahigh vacuum (UHV) environment with the base pressure lower than 10^{-7} Pa. Figure 2.2 shows a schematic representation of UHV experimental setup including sample preparation and characterization. N-doped graphenes were synthesized on Pt (111) by single-source CVD at low-pressure (LPCVD). A platinum substrate was mechanically polished and then cleaned with sonication in acetone for 30 min. A clean Pt (111) surface was prepared through repeated cycles of 3 kV Ar ion bombardment and annealing at 1000 °C in UHV. Cleanness of the Pt (111) surface was confirmed by low energy electron diffraction (LEED) and X-ray photoelectron spectroscopy (XPS). In the LPCVD process, the ways of exposing source molecules to Pt (111) surface are different from liquid and solid sources. For four liquid sources: quinoline, pyridine, pyrrole and pyrimidine, the Pt (111) substrate kept at a desired temperature was exposed to the ambience of source molecules,

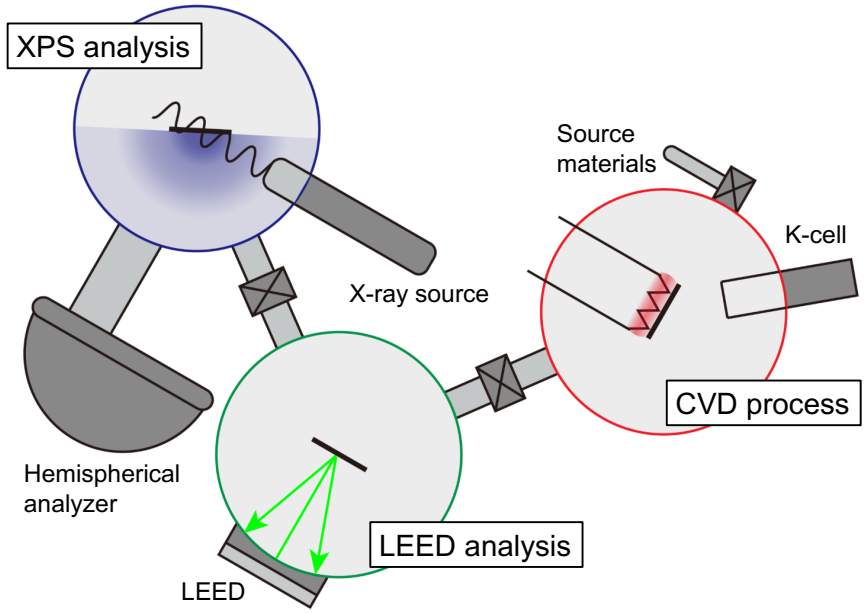

Figure 2.2 Schematic illustration of the *in-situ* experimental setup

which were introduced into the UHV chamber through a variable leak valve. The pressure was kept at 0.1 Pa for 60 min which supplied a sufficient amount of source molecules for obtaining monolayer graphene with the full coverage. For two solid sources: methyl-form and ketone-form, both molecules were evaporated from a Knudsen cell in the UHV chamber to a heated substrate. The deposition rate was set to be 0.16 Å/s which was monitored with a quartz crystal microbalance (QCM). The deposition was continued until the total flux on Pt amounted to 30 nm by QCM. The temperature of the substrate (T_s) was determined with an infrared pyrometer at high temperatures and a thermocouple at lower temperatures. The as-grown films were transferred to the analysis chamber without breaking vacuum and characterized by *in-situ* XPS and LEED measurements. XPS measurements were performed by using Mg Kα radiation (1253.6 eV) (Thermo VG Scientific XR3E2) as an X-ray source and photoelectrons were analyzed by a hemispherical analyzer (SPECS, PHOIBOS-100). LEED measurements were performed by a BDL800IR-MCP2 spectrometer (OCI Vacuum Microengineering Inc.) with a beam energy of 100 eV. After the XPS and LEED measurements, the film was transferred to a SiO_2 substrate by a bubbling method[42] and characterized with Raman spectroscopy in the air. The Raman spectrum was measured by NRS-3100 (JASCO Corporation) with an excitation wavelength of 532 nm. Figure 2.3 shows a picture of Pt (111) single-crystal substrate and as-transferred graphene/poly(methyl methacrylate) (PMMA) on SiO_2 substrate. The Raman spectrum of single-layer graphene on Pt (111) substrate is suppressed and weakened by interaction with the substrate (Figure 2.4(a)). Therefore, it is highly demanded to transfer graphene to other inert substrates, such as SiO_2. Before the Raman measurement, PMMA which covers the graphene was removed with acetone in advance. Figure 2.4(b) shows Raman spectrum of as-transferred graphene on SiO_2 substrate. The signal intensity is drastically improved after the transfer, even for the shorter exposure time on laser excitation.

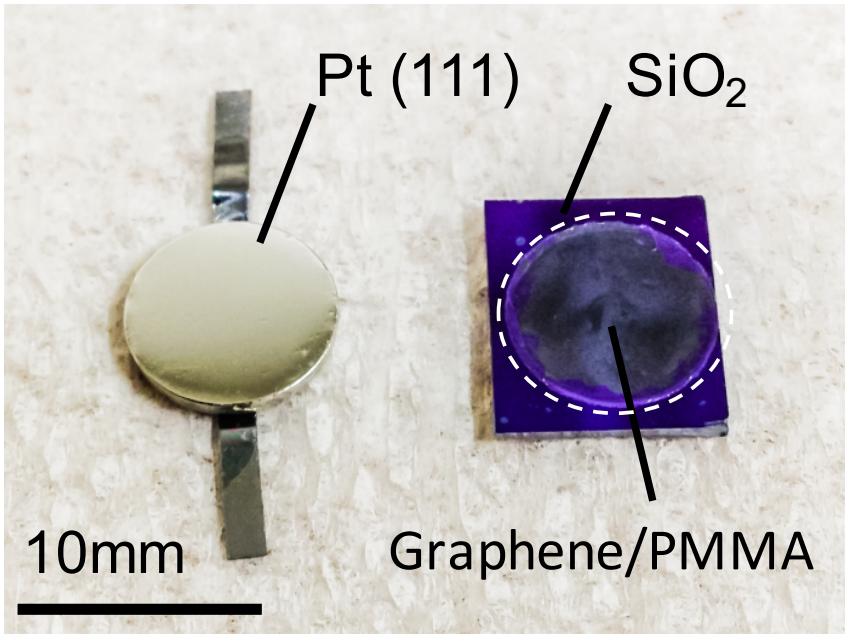

Figure 2.3 Photograph of Pt (111) single-crystal substrate (left) and as-transferred graphene/poly(methyl methacrylate) (PMMA) on SiO_2 (right). Graphene was synthesized from benzene at 400 °C.

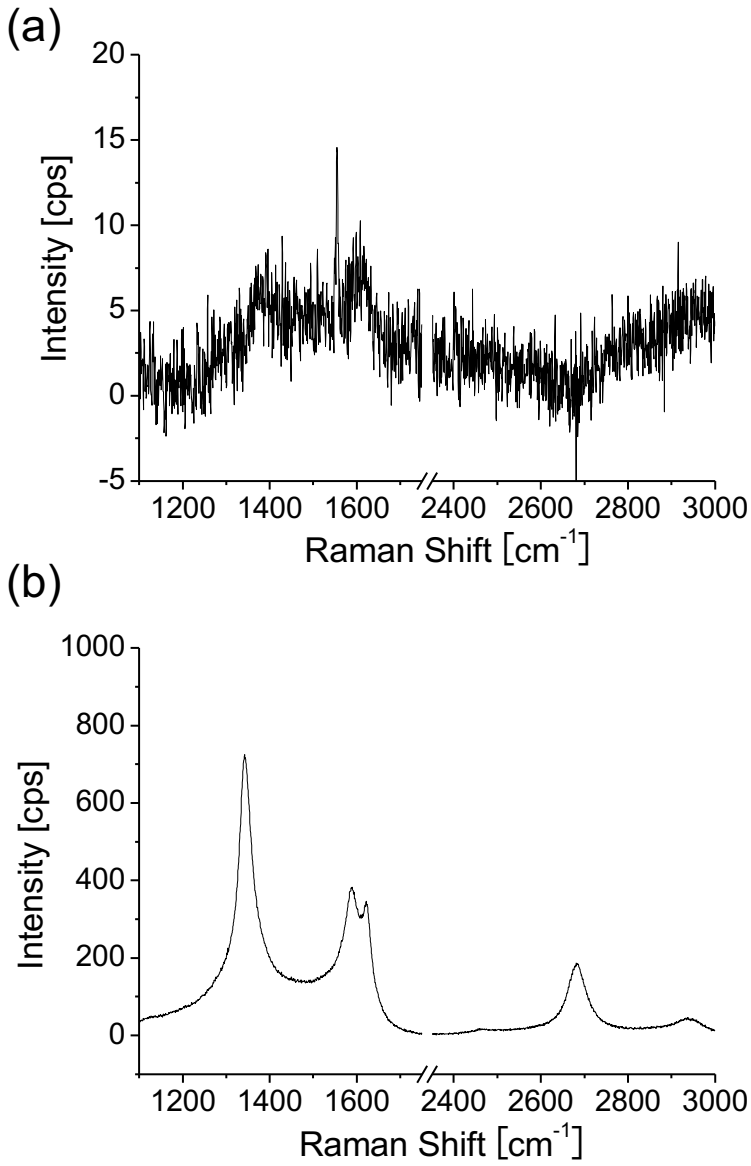

Figure 2.4 Raman spectrum of graphene on (a) Pt (111), and (b) SiO_2 substrate. Graphene was prepared from benzene at 400 °C. The exposure time was 30 s for graphene on Pt (111) and 10 s for SiO_2. Excitation wavelength (532 nm) and a number of scans (3 times) are the same for each sample.

2.3 Synthesis of pyridinic- and pyrrolic-nitrogen-doped graphene from nitrogen-containing aromatic compounds

2.3.1 Results

First, N-doped graphene was synthesized on Pt (111) kept at 500 °C. Figure 2.5 shows the LEED patterns of the films deposited at 500 °C from the source molecules: (a) quinoline, (b) pyridine, (c) pyrrole, and (d) pyrimidine. Two noticeable features are observed in the diffraction patterns; sharp spots with six-fold rotational symmetry, and arc-shaped spots with twelve-fold rotational symmetry. The sharp spots with six-fold symmetry originated from the Pt (111) surface. The arc-shape spots outside the Pt spots

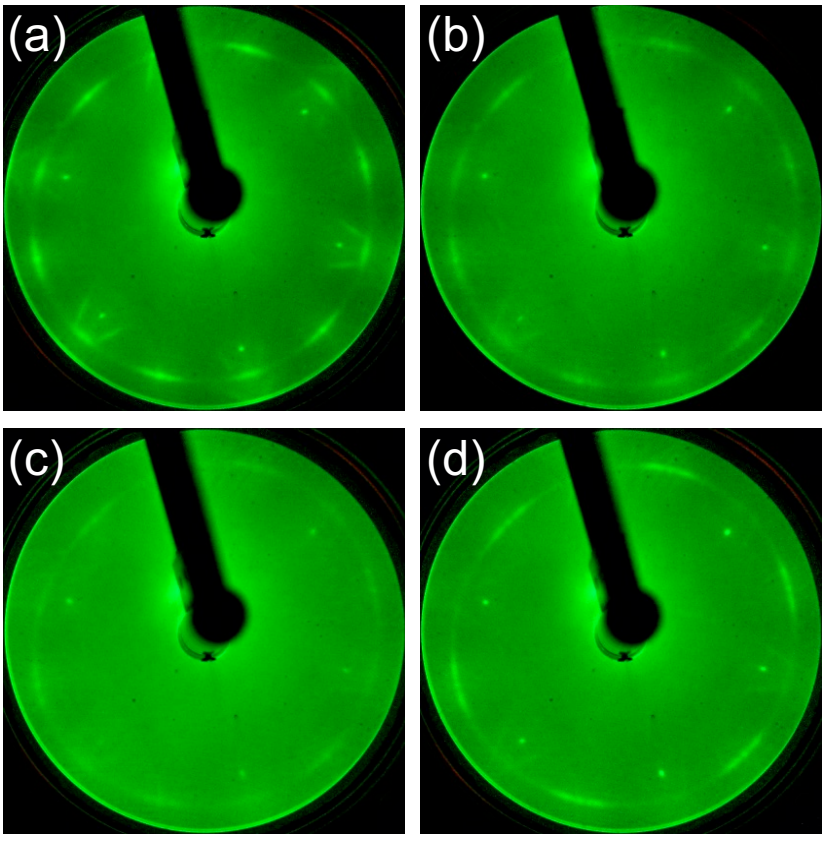

Figure 2.5 LEED patterns of the films synthesized at 500 °C from (a) quinoline, (b) pyridine, (c) pyrrole, and (d) pyrimidine.

were previously observed for the graphene on Pt.[43] The lattice constant of 2.46 Å calculated from the radius of arc-shape spots in Figure 2.5 is equal to that of graphene (2.46Å). Arc-shaped patterns oriented 0° and 30° with respect to Pt spots exhibits the weak epitaxial growth of graphene. It indicates that weakly ordered or oriented grains of graphene are formed on Pt (111) substrate. The diffraction spots from graphene were observed for all the films synthesized at 500 °C. The intensity of the arc-shape spots depends on the source molecule. The arc-shape spots are sharp for the quinoline-derived graphene (Figure 2.5(a)), whereas that are blurred for the pyrrole-derived graphene (Figure 2.5(c)). The difference in sharpness reflects the domain (grain) size of graphene. The term of domain size implies an expanse of an sp^2 hybridized carbon network of graphene. Judging from the intensity of the arc-shape spots and the moiré structures around Pt spots, the domain size increases in sequence, pyrrole, pyridine, pyrimidine, and quinoline.

Raman spectroscopy is a powerful method for evaluating the structure of graphene. Figure 2.6 shows the Raman spectra of the graphenes synthesized from four kinds of molecules at 500 °C. The G band at ~ 1580 cm^{-1} originates from the sp^2 carbon network. The D band located at ~ 1350 cm^{-1} indicates the presence of a certain amount of defects in the sp^2

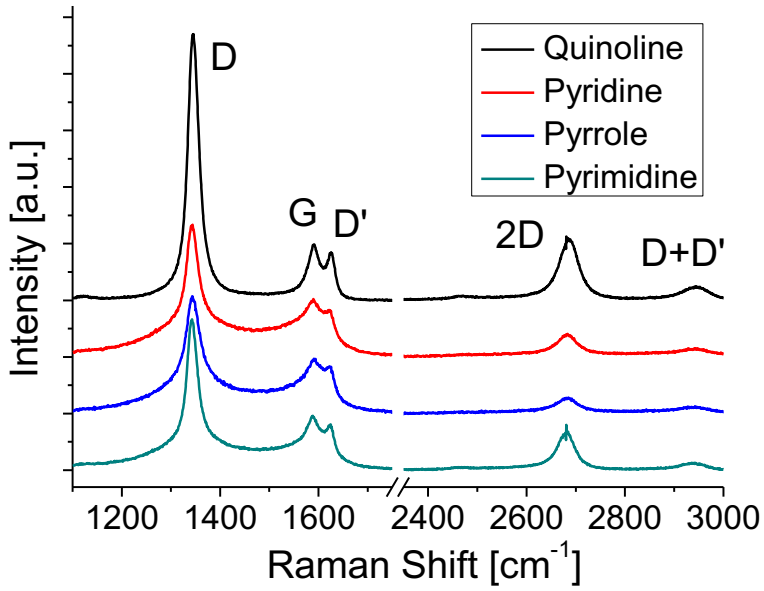

Figure 2.6 Raman spectra of N-doped graphenes synthesized at 500 °C.

carbon network.[44] In addition, a component for amorphous carbon is identified between the D band and the G band.[45,46] The D' band at ~1620 cm^{-1} is also activated by defects in graphene and enhanced especially by boundaries and vacancies.[47] The spectra showed in Figure 2.6 are normalized with the peak height of the G band. The absence of amorphous components (between D and G bands) in the quinoline-derived graphene indicates its largest domain size of the four. For the graphenes synthesized from the other source molecules, the intensity of the 2D band (~ 2700 cm^{-1}) might be a good index to evaluate the domain size of the graphene; the more I_{2D}/I_G is, the larger the domain size is.[48,49] Judging from the Raman spectra, the domain size of the N-doped graphene increases in sequence, pyrrole, pyridine, pyrimidine, and quinoline, which is consistent with the results of LEED measurements (Figure 2.5).

The amount and chemical state of nitrogen in graphene was evaluated by XPS measurement. The absence of oxygen atom was confirmed for all the specimens by the XPS in the O 1s region. Figure 2.7 shows the XPS spectra in the region of N 1s for the graphenes synthesized from (a) quinoline, (b) pyridine, (c) pyrrole, and (d) pyrimidine at 500 °C. Each of the spectra was fitted with three Gaussian functions, which corresponded to pyridinic- (398.6 eV), pyrrolic- (400.1 eV), and graphitic- (401.0 eV) N states. The component at around 402 eV can be assigned to positively charged nitrogen since there is no oxygen detected in XPS measurement (Figure 2.8).[50] The nitrogen content, defined as [N]/([C]+[N]), was evaluated from the areas of the N 1s and the C 1s peaks. The quinoline-derived graphene (Figure 2.7(a)) is dominated by pyridinic-N (0.35 %). The pyridine- and pyrimidine- derived graphenes, on the other hand, consist of both pyridinic- and graphitic-N states (Figure 2.7(d)). It is noteworthy that the pyrimidine-derived graphene contains less nitrogen (1.78 %) than the pyridine-derived one (2.41 %), even though the N content of pyrimidine is higher than that of pyridine. The pyrrole-derived graphene contains the largest amount of N atoms (4.28 %) doped predominantly at pyrrolic-N sites (Figure 2.7(c)).

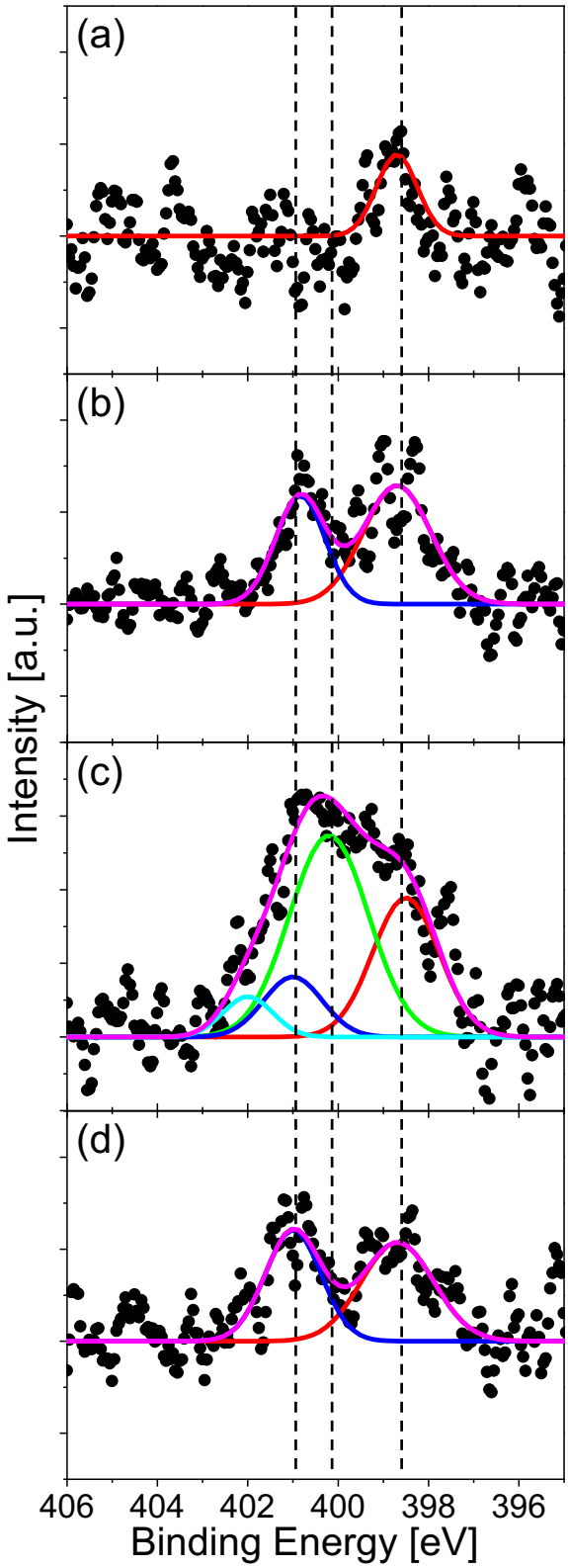

Figure 2.7 XPS N 1s spectra of N-doped graphenes synthesized at 500 °C from (a) quinoline, (b) pyridine, (c) pyrrole, and (d) pyrimidine. Each spectrum is fitted with three Gaussian functions: pyridinic- (red line), pyrrolic- (green line), and graphitic-N (blue line).

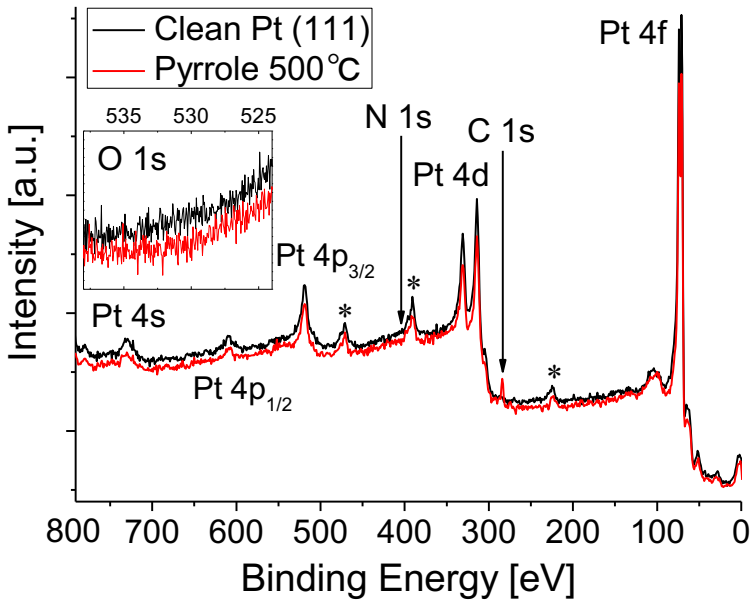

Figure 2.8 Wide range XPS spectra. Inset figure shows XPS O 1s region spectra. *Peaks from Ta used as a substrate holder.

There are several reports which synthesized nitrogen-doped graphene on Cu foil by CVD with using pyridine as source molecule.[30,35] According to these literature, nitrogen-doped graphene with around 2.4 % of N atoms has obtained at 1000 °C. By comparing them with this result, they need twice the temperature (in °C) to synthesize graphene with same N concentration. The difference is considered mainly due to the high catalytic activity of Pt substrate.

XPS measurement revealed that the N content increased in sequence, quinoline, pyrimidine, pyridine, and pyrrole. This order correlates inversely with that of the domain size evaluated from the sharpness of LEED and the 2D intensity of Raman spectra. The nitrogen atoms doped into the graphene lattice seemed to decrease the domain size. The nitrogen atom bonded at grain edge would hamper the lateral growth of graphene, leading to the smaller domain size.[32] Therefore, the larger the N content was, the smaller the domain size became.

The incorporation of nitrogen atoms also affected the C 1s spectra. Figure 2.9 shows the XPS C 1s spectra of graphene synthesized at 500 °C. The peak intensity ratio of C 1s to Pt 4f indicates that the as-grown graphenes were a monolayer.[37] A satellite peak observed around 286 eV originated from C-N bonds. The intensity of this peak increases in sequence, quinoline, pyrimidine, pyridine, and pyrrole, which is consistent with the N content determined from N 1s spectra.

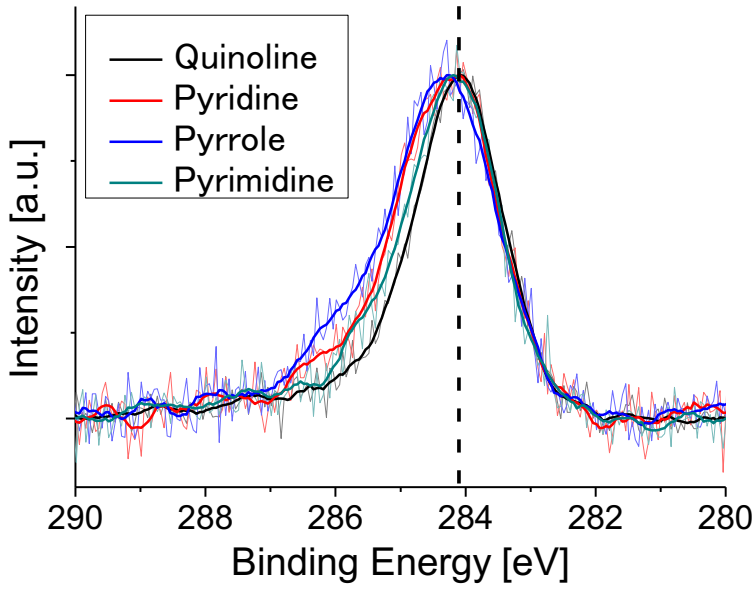

Figure 2.9 XPS C 1s region spectra of the graphenes synthesized at 500 °C. The dashed line at 284.1 eV is attributed to the sp^2 carbon of graphene.

In order to investigate the growth mechanism of N-doped graphene, the growth temperature was changed. Figure 2.10(a) shows the XPS N 1s spectra of the graphenes synthesized from the source molecules: quinoline, pyridine, pyrrole, and pyrimidine at 600 °C. Nitrogen doping was observed only for the pyridine-derived graphene, in which graphitic-N and pyridinic-N peaks are observed with the total N content of 1.64 %. Figure 2.11 shows the C 1s region spectra for the graphenes grown at 600 °C. Only the pyridine-derived graphene shows a broad peak with a shoulder at the higher binding energy side. The graphenes synthesized from other molecules have only a narrow peak at 284.1 eV, indicating the absence of nitrogen in the graphene lattice. Exclusion of nitrogen atoms during the CVD growth suggests that source molecules were decomposed and nitrogen-containing fragment was detached from the surface. Figure 2.10(b) shows the temperature dependence of the nitrogen content for each source molecule. At 600 °C, N-doped graphene can be obtained only from pyridine. At higher temperature (over 700 °C), LEED and XPS revealed that non-doped graphene was formed regardless of the source molecules.

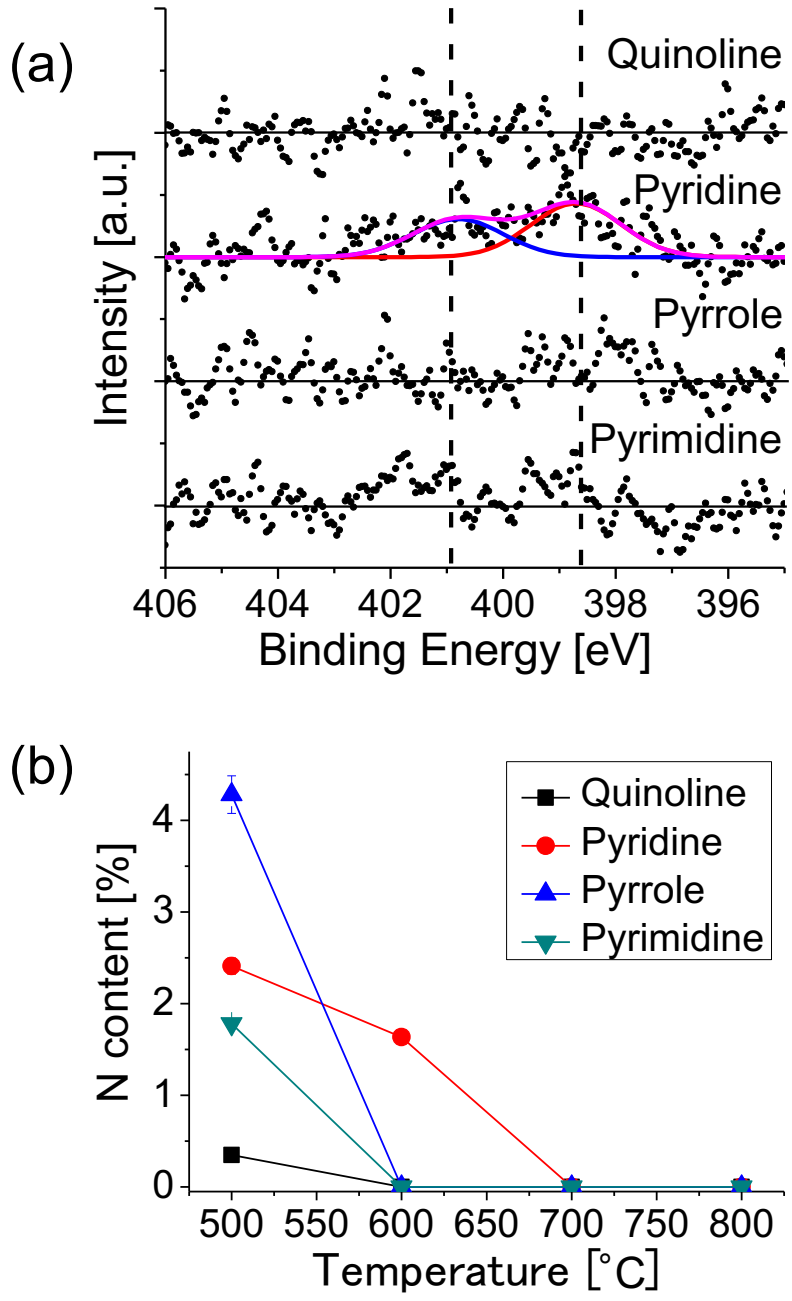

Figure 2.10 (a) XPS N 1s spectra of the graphenes synthesized at 600 °C. (b) Nitrogen content as a function of growth temperature for each of the source molecules.

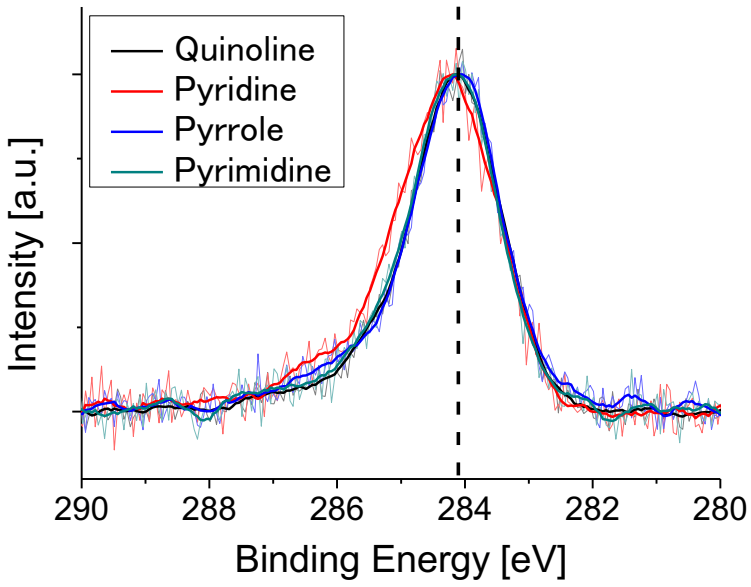

Figure 2.11 XPS C 1s region spectra of the graphenes synthesized at 600 °C. The dashed line at 284.1 eV is attributed to the sp^2 carbon of graphene.

Figure 2.12 shows the Raman spectra of the graphenes formed at 600 °C. Compared to the graphenes formed at 500 °C, the relative intensity of 2D band increases for all the graphenes, which means the increase of the domain size. In the LEED images, the blurred arc-shape spots observed for the graphenes formed at 500 °C (Figure 2.5(c)) become clear

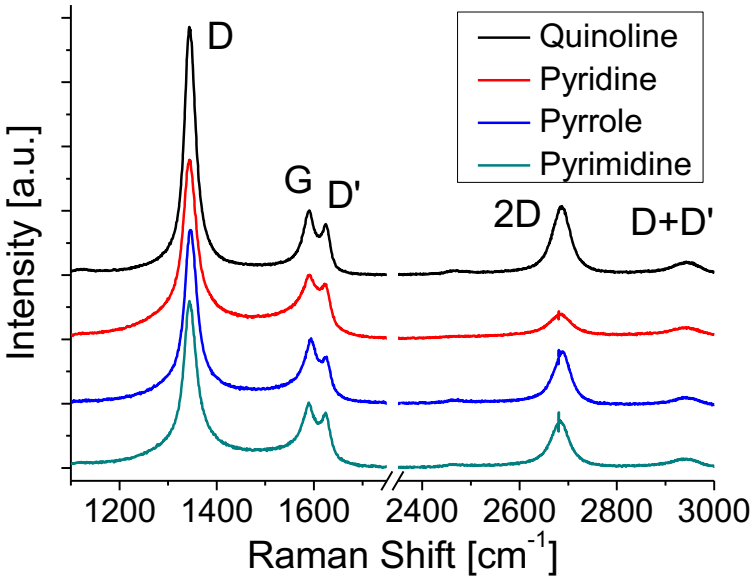

Figure 2.12 Raman spectra of the graphenes synthesized at 600 °C.

six- or twelve-fold symmetrical spots for the graphenes formed at 600 °C (Figure 2.13(c)), which also means the increase of the domain size. At 600 °C, the pyridine-derived graphene shows the smallest domain size of the four. This incorporation of nitrogen atoms impedes the evolution of domain size in the pyridine-derived graphene. The other three samples are free from N-dopants, though 600 °C is not sufficient temperature to produce a large scale and defect-free graphene on Pt by CVD. The domain size of the graphene needs to be larger than the diameter of LEED spot (~ μm) to observe the "spots" of graphene.

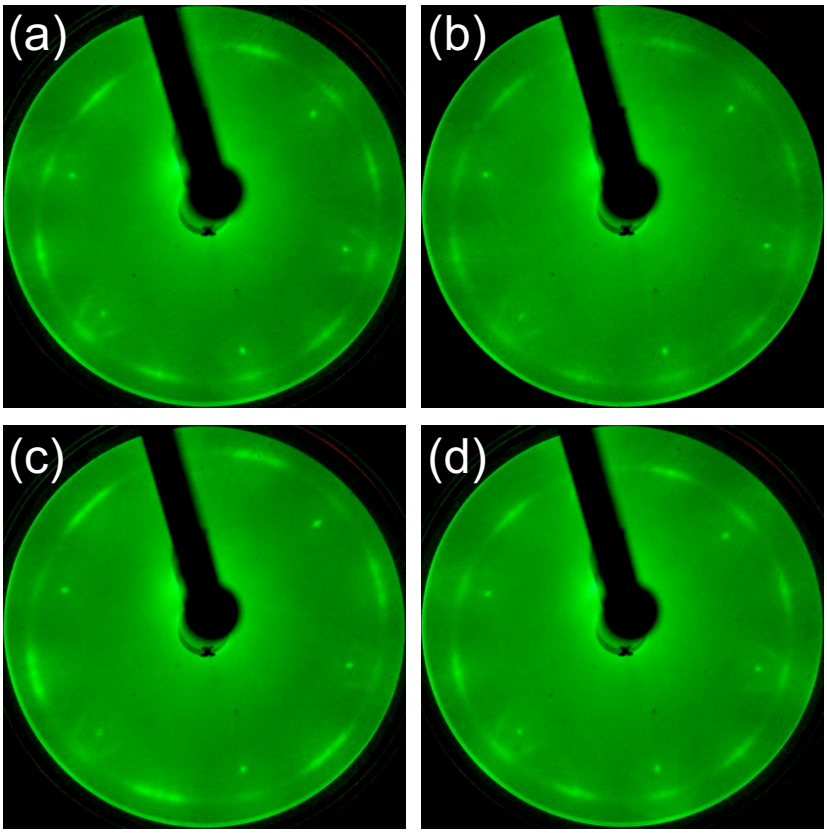

Figure 2.13 LEED patterns of the graphenes synthesized at 600 °C from (a) quinoline (b) pyridine (c) pyrrole (d) pyrimidine.

2.3.2 Discussions

Nitrogen-doped graphene was synthesized from four kinds of aromatic molecules. Table 2.1 summarizes the experimental results: the nitrogen content for the films deposited at

500 °C and 600 °C together with the major doped sites. N_{mole} means the nitrogen content in each molecule. The nitrogen content N_{500} seems increasing with $N_{mole,}$ but it decreases for pyrimidine. N_{600} is finite only for the pyridine-derived graphene. With respect to doped sites, pyrrole-derived and quinoline-derived graphenes have a single kind of the site, while two kinds of site are observed for pyridine-derived and pyrimidine-derived graphenes. In this section, the growth mechanism of nitrogen-doped graphene is discussed focusing on the two points: doped amount and doped site.

The nitrogen content is much smaller than that of source molecule in any case. That means decomposition occurred for the graphene growth even at temperatures as low as the present case. It has been reported that a major component decomposed thermally from these aromatic molecules is HCN.[54,56–58] The CVD process on metal substrates would desorb such a volatile species as HCN from the surface before graphene formation, which resulted in the exclusion of nitrogen atoms from graphene.[36] Some previous works proposed that a bond reforming process play a role for nitrogen atoms to be incorporated into graphene during CVD growth.[36,37] In the bond reforming process, partially decomposed or deformed aromatic molecules coalesce with each other, leading to the formation of graphene.[59,60] Less decomposition might be favorable for the remaining of nitrogen atoms in the synthesized graphene.

The activation energy of ring opening reaction ($E_{C\text{-}N}$) in the aromatic compounds is shown in Table 2.1. The order of remaining nitrogen amount qualitatively agrees with that of

Table 2.1 Nitrogen content of the films N_{500} and N_{600} deposited at 500 °C and 600 °C, respectively. N_{mole} is the N content in the molecule. $E_{C\text{-}N}$ is the activation energy of ring opening reaction. (References of $E_{C\text{-}N}$ are shown as superscript.)

Source molecule	N_{mole}	N_{500}	(N_{500}/N_{mole})	N_{600}	$E_{C\text{-}N}$ [ref] (kJ/mol)	N-doped sites
quinoline	0.100	0.004	0.035	0	188 [51]	pyridinic
pyridine	0.167	0.024	0.145	0.016	320 [52]	pyridinic, graphitic
pyrrole	0.200	0.043	0.214	0	318 [53,54]	pyrrolic
pyrimidine	0.333	0.018	0.053	0	275 [55]	pyridinic, graphitic

decomposition energy. Pyrrole and pyridine have high activation energy and a high nitrogen content among the four molecules. Thus, the number of molecules participating the graphene formation via bond-reforming process is relatively high for these molecules. This relation could explain why the pyridine-derived graphene has a higher amount of nitrogen than the pyrimidine-derived one although the amount of nitrogen is half that of pyrimidine in the molecule.

For the growth at 600 °C, only the pyridine-derived graphene contains the nitrogen in the lattice. The pyrrole-derived graphene grew excluding the nitrogen, although the activation energy of decomposition was close to that of pyridine. This difference could be ascribed to the difference in the intermediate species produced by the ring-opening reaction. A major product of the ring-opening reaction is N-terminated radicals such as •CH=CHCH=CHC≡N. C-terminated radical species such as •CH=CHCH=N−C≡CH are, however, also produced by cleavage of a C-C bond in pyridine.[52,58] Such C-terminated species were less likely to be converted into volatile species and could be attached to the growing graphene edges. At higher temperatures at which most source molecules are decomposed, N atoms could be thus incorporated into graphene synthesized from pyridine.

In contrast, C-terminated species are hardly produced from pyrrole. The activation energy of C-C bond cleavage was theoretically evaluated to be greater than that of the C-N bond by 164 kJ/mol for pyrrole,[61] while only 31.5 kJ/mol for pyridine.[52] Thus C-terminated radical species are rarely produced from pyrrole at 600 °C, while partly produced from pyridine at the same temperature. Thus, it can be concluded that the thermal stability of source molecules affects the doped amount strongly in the graphenes synthesized from N-containing aromatic molecules.

Nitrogen atoms were incorporated mostly via bond reforming process, and thus the doped site tended to reflect the site the nitrogen atom occupied in the source molecule. Nitrogen atoms resided at a pyridinic site and a pyrrolic site in the quinoline-derived graphene and pyrrole-derived graphene, respectively. Pyridine- and pyrimidine-derived graphenes,

however, had graphitic nitrogen atoms in addition to pyridinic ones. It is considered that the presence of graphitic-N is due to the structural affinity of pyridine and pyrimidine for the honeycomb lattice of graphene. These two molecules can be easily incorporated into graphene lattice due to their hexagonal molecular shape. Such structural affinity increases the probability of the formation of graphitic-N during the coalescent process.[27,31,34] In contrast, it is difficult for pyrrole to be incorporated into the inside of the honeycomb lattice of graphene retaining their original molecular shape. Because of its low structural affinity, a pyrrole molecule can only be incorporated at the edges of graphene, terminating the growth of graphene by pentagonal edges. With focusing on the skeletal structure, quinoline has only two-fold symmetry, whereas pyridine and pyrimidine have six-fold symmetry. Due to such lower structural symmetry and larger molecular size of quinoline, the probability of coalescence in the bond-reforming process might be smaller than those of pyridine and pyrimidine. Therefore, quinoline was not incorporated into the inside of graphene, but at the edge of graphene domains, resulting in the dominant pyridinic-N doping with lower N concentration.

These discussions showed that there is a trade-off relation between the formation and N-doping of graphene in this method, and the structural incompatibility of source molecule is the key for the site-selective N-doping to graphene. Preservation of molecular structure is essential for the site-selective N-doping to reflect its structure to graphene, but graphitization will not occur unless molecules are decomposed. Thermally persistent precursors are effective for a large amount of N doping. However, they tend to terminate the graphene growth. In fact, the domain size of graphene increased, as the N content decreased. Thus, the structural affinity and the thermal stability are needed to be considered when choosing the source molecule. Further, it can be expected that sites and the amount of N-doping can be controlled with the appropriate selection of the source molecule.

2.4 Synthesis of graphitic-nitrogen-doped graphene from nitrogen-embedded cyclic triarylamines

N-doped graphene with dominant pyridinic-N and predominant pyrrolic-N was successfully synthesized from source molecules with two-coordinated N atom in the previous section. However, synthesis of exclusively graphitic-N doped graphene remains challenging. In this section, methyl-form and ketone-form which are molecules with three-coordinated N (graphitic nitrogen atom) were used aiming to fabricate such N-doped graphene. Each of these molecules was deposited as a source molecule to prepare graphene on a heated Pt (111) substrate (see section 2.2.2).

2.4.1 Growth from methyl-form

The film derived from the methyl-form was characterized by LEED *in-situ*. The film deposited at RT showed no structure other than the six-fold spots of Pt (111) substrate. Figure 2.14 shows the LEED patterns of the film fabricated on Pt (111) at different T_s: (a) 300 °C, (b) 400 °C, (c) 500 °C. The six-fold sharp spots of the Pt (111) substrate were observed regardless of T_s. For the film grown at 300 °C, a faint ring structure was observed outside the six LEED spots of the Pt (111) surface as shown in Figure 2.14(a). From the diameter of the ring, the diffraction pattern can be ascribed to the graphene with

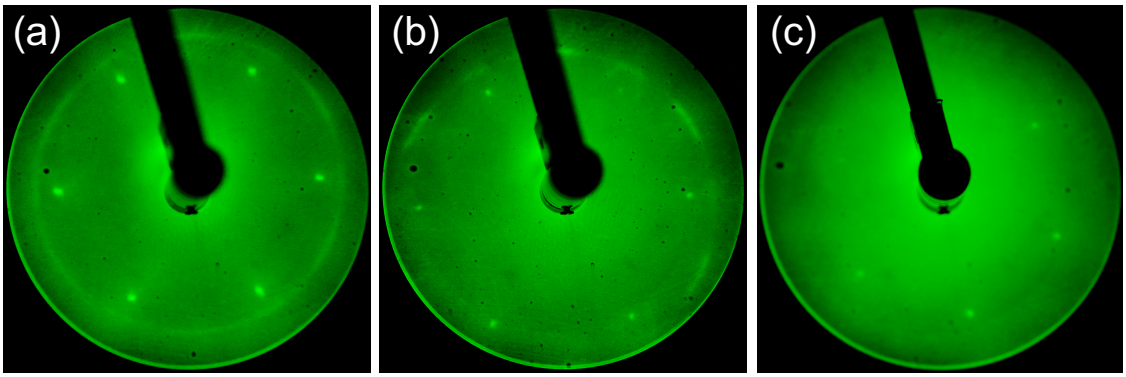

Figure 2.14 LEED patterns of the film fabricated with depositing methyl-form on Pt (111) at (a) 300 °C, (b) 400 °C, and (c) 500 °C. The beam energy was 100 eV.

a high degree of rotational disorder. When the T_s was increased to 400 °C, the ring pattern changed into the arc-shaped pattern as shown in Figure 2.14(b). The centers of the arcs are rotated by 30° with respect to the first order Pt spots. The arcs with 30° rotation were also observed for the graphene grown on Pt (111) at high temperatures.[43] When the T_s was further increased to 500 - 600 °C, the arcs disappeared, and only the Pt-derived spots were observed as shown in Figure 2.14(c).

The deposited film was characterized by XPS to study the atomic concentration and the chemical state. Figure 2.15 shows the wide-scan XPS spectra of Pt (111) before and after the deposition of methyl-form molecules at 400 °C. Several peaks which can be ascribed to Pt-derived lines were found. After depositing the methyl-form molecules, the C 1s peak appeared around the binding energy of 284 eV. Figure 2.16 shows the C 1s region spectra (Figure 2.16(a)) and the C coverage which can be represented as an intensity ratio of C 1s (I_C) to Pt 4f (I_{Pt}), as a function of T_s. The amount of deposited carbon atoms decreases with increasing T_s. It is known that the monolayer graphene on Pt (111) shows the

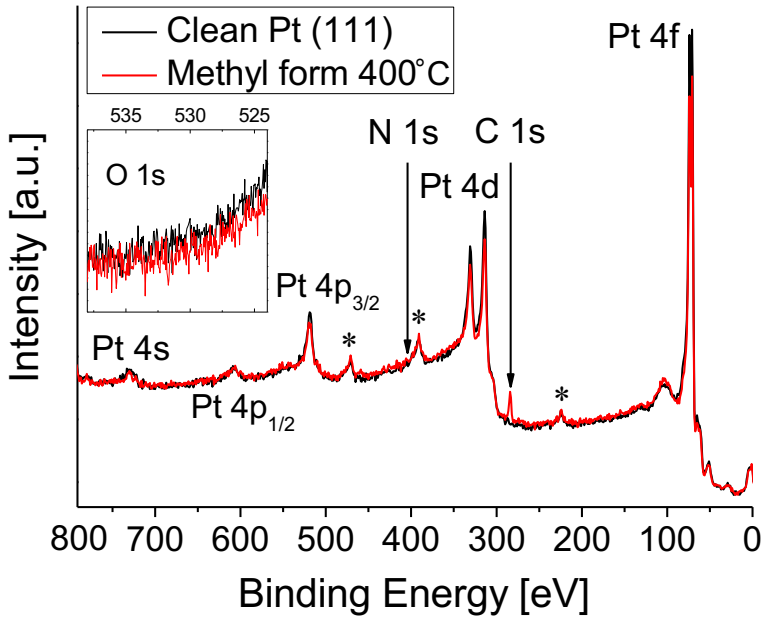

Figure 2.15 Wide range XPS spectra of clean Pt (111) surface and methyl-form derived films at 400 °C. The inset figure shows O 1s region spectra. *Peaks from Ta used as a substrate holder.

intensity ratio of 0.034.[37] Therefore the amount of C atoms in the film deposited at 400 °C is well agreed to that of monolayer graphene.

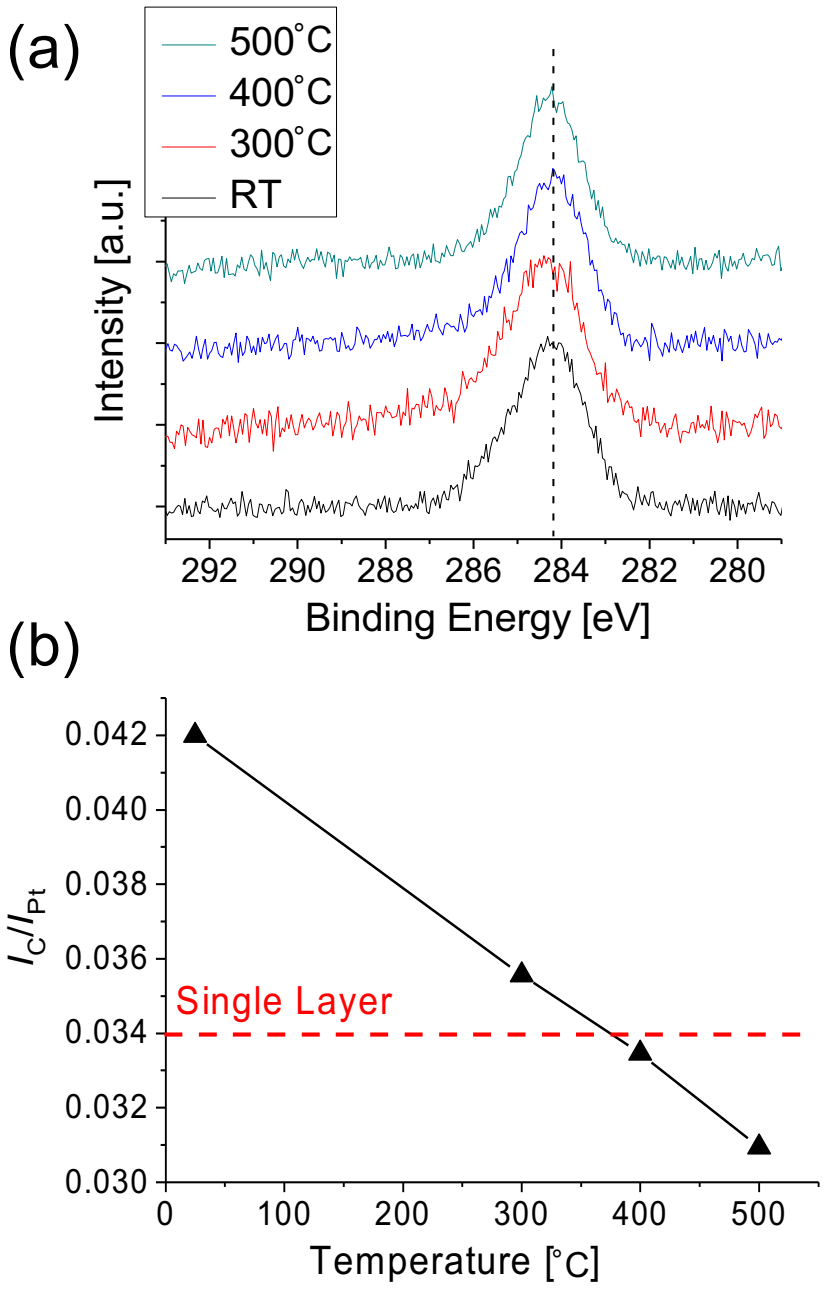

Figure 2.16 (a) XPS C 1s region spectra of methyl-form derived films at various T_s, (b) T_s dependence on coverage of carbon atom. The coverage was estimated from the intensity ratio of C 1s (I_C) to Pt 4f (I_{Pt}),

High-resolution spectra in the energy region of N 1s electrons are shown in Figure 2.17(a). The film deposited at RT has a peak centered at 400.0 eV. The nitrogen concentration is estimated to be 3.2 %, which is close to the value of 3.7 % in a methyl-form molecule within an accuracy of atom sensitivity factors. The film deposited at 300 °C has the

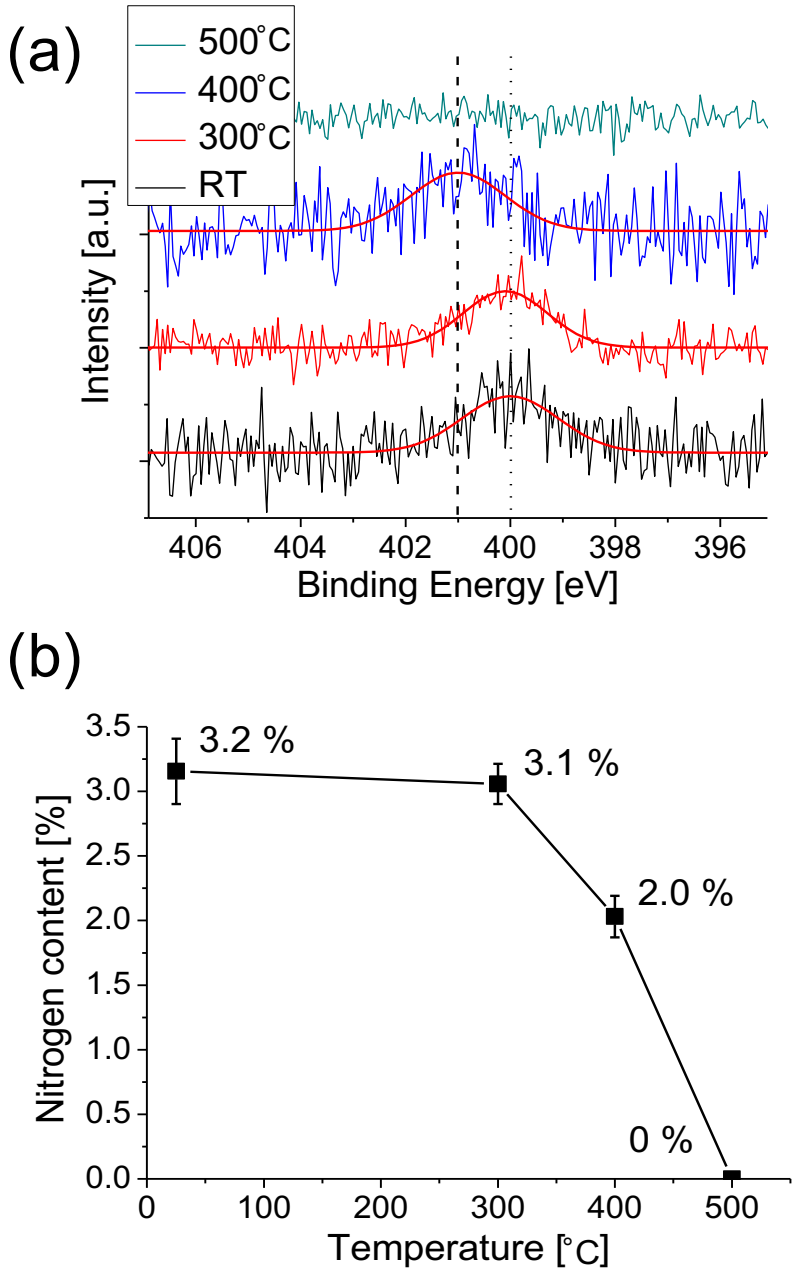

Figure 2.17 (a) XPS N 1s region spectra of methyl-form derived films at various T_s, (b)Temperature (T_s) dependence of nitrogen concentration.

binding energy and the nitrogen content almost like those at RT. For the film deposited at 400 °C, the N 1s peak was observed at 401.0 eV, and the concentration decreased to 2.0 %. For the film deposited at T_s higher than 500 °C, no trace of N was discerned. Figure 2.17(b) shows the nitrogen concentration as a function of T_s.

Figure 2.18 shows the Raman spectra of the films deposited at various T_s. The film deposited at RT could not be transferred to SiO_2, meaning reactions that produce large polymers did not occur. The spectrum of 300 °C shows broad and blurry peaks around 1350 and 1600 cm^{-1}, which are assigned as the D and G bands characteristic of carbon-based materials. There is no evidence of the formation of an sp^2 network, and the spectrum is much more like amorphous carbon films rather than graphene. In the spectrum of 400 °C, on the other hand, the D and G bands were sharpened, and a sharp 2D band appeared around 2700 cm^{-1}, indicating the formation of a large network of sp^2 carbon atoms. The D' peak was slightly observed as a shoulder of G band. Also, the peak appeared around 3000 cm^{-1}, which is associated with D+D' peak.[62] The spectrum of 500 °C again showed broad D and G bands together with the disappearance of the 2D

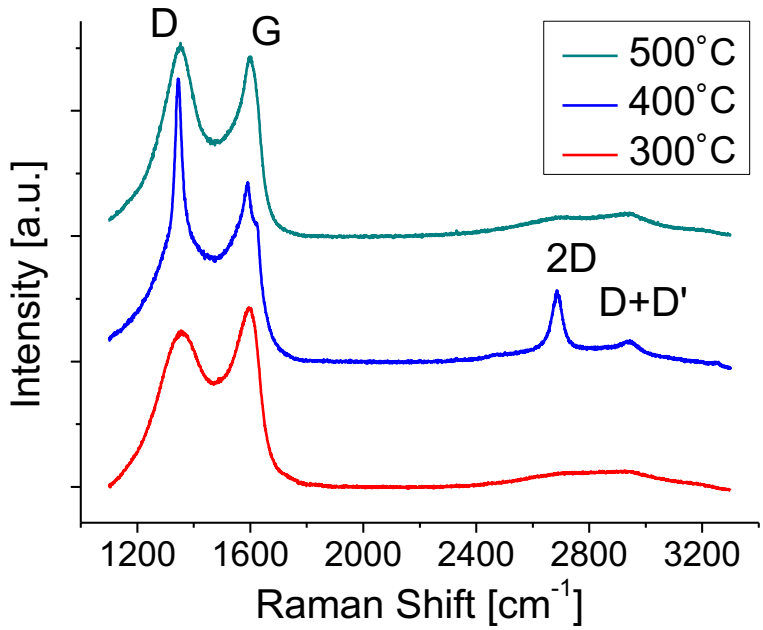

Figure 2.18 Raman Spectra of the methyl-form film deposited on Pt (111) at various T_s and transferred onto SiO_2 substrate.

band. From the Raman spectra, it was found that the graphene lattice was formed only at T_s of 400 °C.

2.4.2 Growth from ketone-form

To explore the effect of the difference in the peripheral structure on the extent of graphitization and nitrogen doping, the ketone-form compound was also deposited on the Pt (111) surface at various T_s. Figure 2.19 shows the Raman spectra of the deposited films after being transferred onto SiO_2. The broad G and D bands are observed for the films of 300 °C and 400 °C. For the film deposited at 500 °C, the G and D bands become sharp, and the D', 2D and D+D' band appears.

Figure 2.20 shows the high-resolution XPS spectra in the region of N 1s for the films deposited at various T_s. A single peak centered at 401.7 eV was observed for the film fabricated at RT. The nitrogen content was 4.1 %, which is close to that of the ketone-form molecule (4.7 %). For T_s of 300 °C, the nitrogen content decreased to 1.0 %, and the N 1s peak shifted to a lower binding energy side and split into two components. Figure

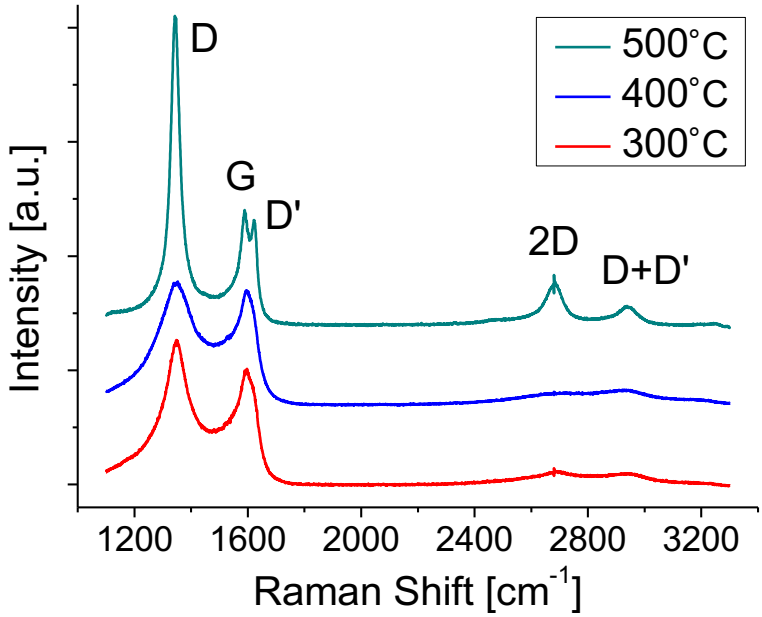

Figure 2.19 Raman Spectra of ketone-form films deposited at different T_s and transferred onto SiO_2 substrate.

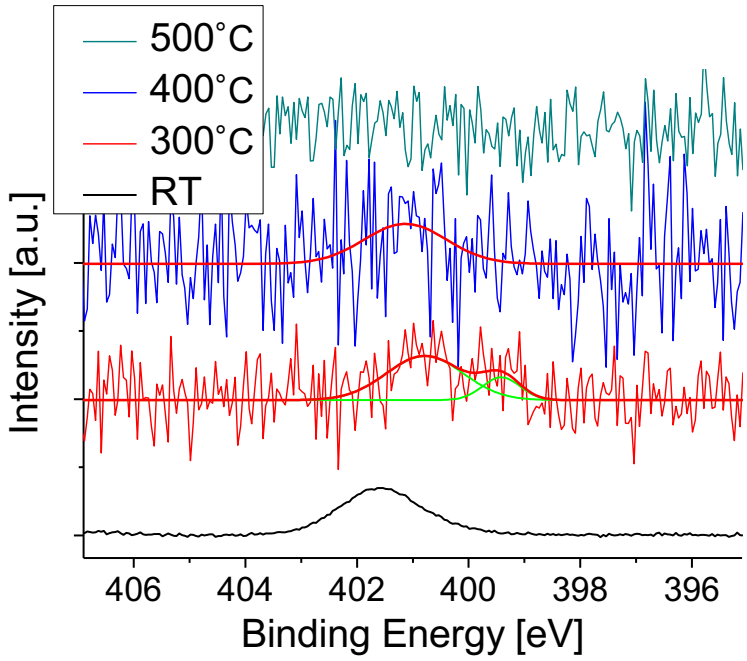

Figure 2.20 XPS spectra in N 1s region of ketone-form derived films at various T_s.

2.21 shows the XPS C 1s region (Figure 2.21(a)) and O 1s region (Figure 2.21(b)) spectra of the same film as shown in Figure 2.19. The C 1s spectrum at RT consists of two peaks at 287.2 eV and 285.3 eV. The peak at the higher energy one can be assigned to the C-O bonding. Only a single peak was observed for the films when elevating the temperature, indicates that C-O bond was decomposed at 300 °C. The O 1s spectrum at 300 °C shows that no oxygen atom was detected in the film. Simultaneously, the C 1s peak split into two components at RT changed into a single component at 300 °C, and the O 1s peak disappeared at all. These results indicate that the molecule decomposed above T_s of 300 °C. At 400 °C, a weak single peak was observed with the concentration of 0.4 %. For T_s higher than 500 °C no trace of nitrogen was observed within the S/N ratio of XPS spectrum.

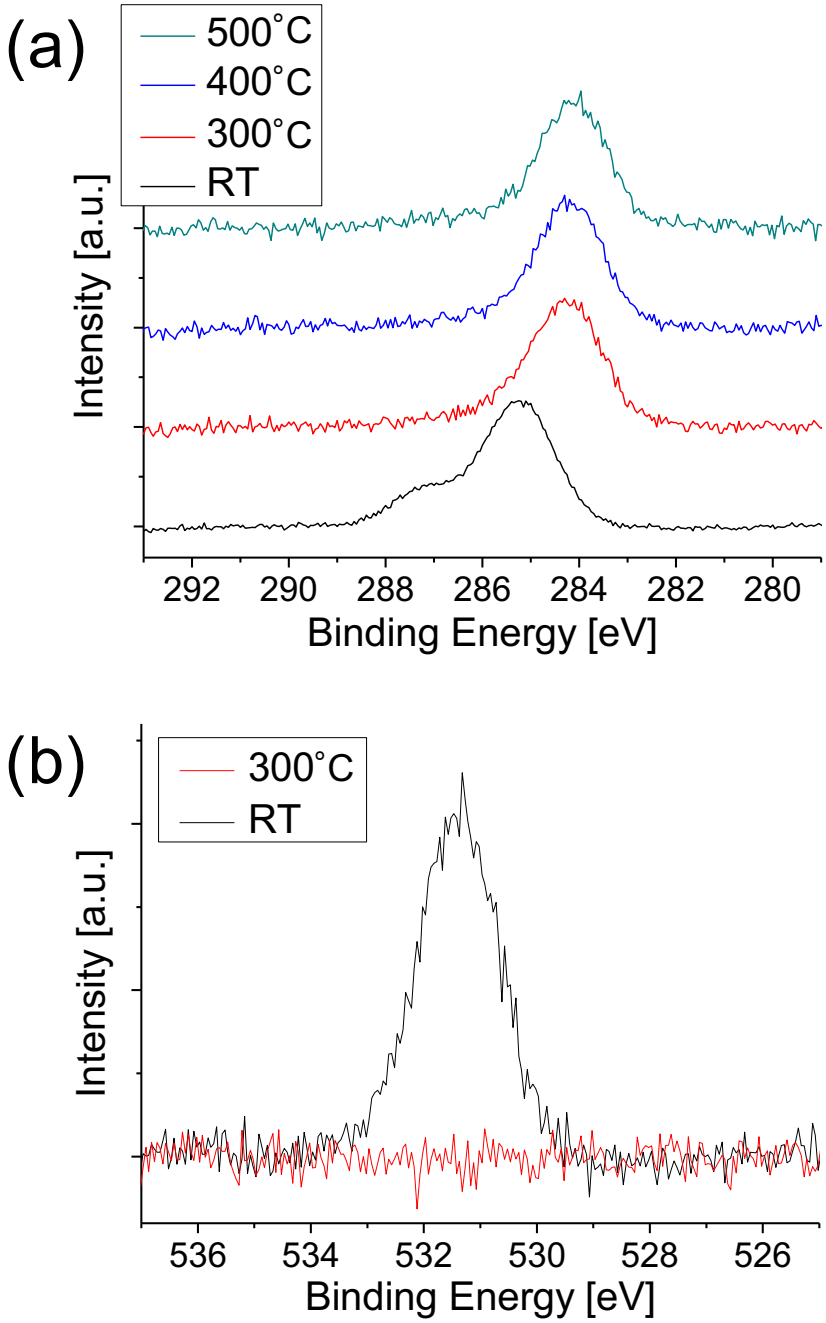

Figure 2.21 (a) XPS C 1s region spectra of ketone-form derived films at various T_s, (b) O 1s region spectra of films fabricated from ketone-form at RT and 300 °C.

2.4.3 Discussions

On the basis of characterization by LEED, XPS and Raman spectroscopy, the growth mechanism of nitrogen-doped graphene from the methyl-form and ketone-form molecules is discussed. At first, the mechanism of the film derived from the methyl-form molecule was considered. For T_s of 300 °C, the position and the shape of XPS N 1s peak was almost unchanged from the spectrum at RT. In addition, N content of the film was only decreased slightly (0.1 %) from the thin-film of methyl form. The result from XPS measurement indicated that the original structure of methyl form is largely retained at 300 °C. In contrast, the LEED pattern (Figure 2.14(a)) shows an outer ring, indicating the formation of graphene-like grains oriented randomly with respect to one another.[43,63,64] The Raman spectrum in Figure 2.18, however, corresponds to an amorphous-like carbon film. Diffraction patterns originating from the periodicity of atomic arrangement would appear for the nano-scale grains even if they are partially formed in the film. The absence of a graphene-like G-band and 2D band in the Raman spectrum, on the other hand, suggests that π-conjugated electronic structure was not formed in the film deposited at 300 °C.

From these results, the structure model as shown in Figure 2.22(a) was proposed. The formation of a solid film transferrable to another substrate suggests that some of the methyl groups in the source molecules had been removed and that the triangle cores were instead bound with each other between the originally dimethylated carbon atoms by a single bond. Several studies have reported such reactions where aromatic precursors coalesce with each other because of intermolecular C-C coupling.[59,65,66] The remaining part of the molecules would stay intact with the chemical state of the central nitrogen atom unchanged, resulting in no chemical shift in the N 1s peak. The region in which the triangle cores are bound in the plane would give rise to the diffraction corresponding to the graphene-like periodicity, but no G-band and 2D-band are coming from the π-conjugated structure. In the figure, the part of triangle cores is not parallel to the surface owing to the steric effect of partially remaining methyl groups.

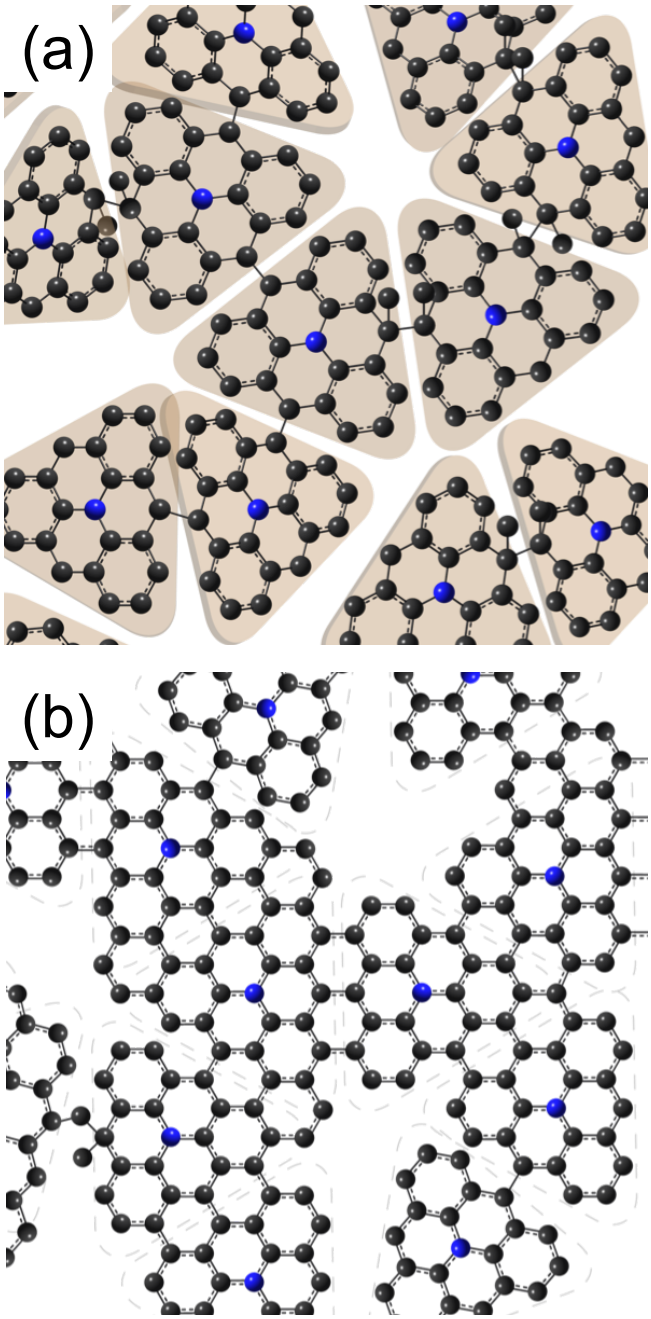

Figure 2.22 Schematic illustration of a possible structure formed from methyl-form molecule at different T_s: (a) 300 °C, (b) 400 °C, respectively. (a) The core structure of the molecule is randomly bonded with each other by a single bond. The core of the molecule is surrounded by beige-colored 3D triangle to clarify and emphasize its 3D orientation. Part of triangle cores is out of the plane. (b) Graphene is formed with the core of the molecule as the basis. The triangle core of the molecule is presented as a dotted line. Single bond links around the N atom in the core structure turn into the π-conjugated network keeping the nitrogen at a quaternary site.

When the T_s was increased to 400 °C, the G and 2D bands characteristic to the graphene lattice appeared, indicating the formation of π-conjugated structures. At this stage, the source molecules would more tightly coalesce via a similar reaction to dehydrogenation and C-C bond formation (Figure 2.22(b)) as reported in several studies.[59,65–68] A large hump between G and D peaks in the Raman spectrum indicates the existence of the considerable amount of amorphous carbon region, and the large D intensity together with the appearance of D' indicates many defects and the small grain size.[44,47] The shift in the binding energy of the N 1s peak to 401.0 eV also indicates such fusion, since the quaternary N has a binding energy of 401.0 eV.[12,15,16,27,28] Single bond links around the N atom in the core structure of methyl form were turned into the π-conjugated network keeping the nitrogen at a quaternary site (graphitic-N). The selective appearance of graphitic nitrogen, which has been scarcely observed previously,[16] is a distinct characteristic of the nitrogen-doped graphene originating from the methyl-form molecule. Therefore, graphitic-N doped graphene was formed with the core of the methyl form as the basis. In the figure, the original triangle core of the molecule is presented as a dotted line.

When T_s was increased further to 500 °C, the Raman spectrum again indicates the amorphous carbon film. The degree of graphitization decreased with increasing T_s, which is in sharp contrast with the CVD growth of graphene from small molecules such as methane.[69,70] If the decomposition of molecules generates carbon species to form graphene, the higher temperature would enhance the graphitization.[36] The present model, however, does not mean the complete decomposition but the partial decomposition such as the removal of methyl groups (Figure 2.17(a)). At T_s higher than 500 °C, decomposition is considered to proceed to the extent that the molecule could not keep its flatness.[59,67] Nevertheless the remaining carbon fragments decomposed at 500 °C are not so small as those that decomposed from methane at a higher temperature. It seems difficult for such large fragments to form graphene via significant reorganization at 500 °C. The absence of nitrogen would come from the fact that the nitrogen-containing fragments rapidly evaporate due to their higher volatility.[36] Thus, it can be concluded that

an amorphous carbon film was grown due to the production of fragments inappropriate for graphitization at 500 °C. The discussion above also supports the growth model depicted in Figure 2.22 in a sense that the methyl-form molecules partially decompose and are bound to each other.

The behavior of the ketone-form is very different from that of the methyl-form. Ketone-form could not form nitrogen-doped graphene at any temperature. The O 1s peak disappeared even at 300 °C (Figure 2.21(b)), and the N 1s peak reduced and split into two components, which indicate the decomposition of the molecules. Transition metal surfaces including Pt are well known to facilitate decarbonylation of carbonyl compounds.[71–74] It seems that the interaction with a Pt surface removed C-O from the ketone-form molecules at a temperature as low as 300 °C. Thus, it can be supposed that oxygen is desorbed as carbon monoxide to lose the original highly rigid structure. Although there are no exact ideas about chemical species formed at 300 °C, the formation of more flexible species bearing no or less peripheral carbonyl linkers might occur. The flexible species would be much easier to decompose further with the loss of nitrogen. This loss of nitrogen would lead to the formation of graphene lattice with a smaller content of nitrogen. The ketone-form molecule is almost completely decomposed at 500 °C and produces benzene or its fragments, leading to the formation of graphene without nitrogen.

2.5 Conclusions

In conclusion, six kinds of nitrogen-containing heterocyclic compounds were selected and deposited on a heated Pt (111) substrate, respectively as precursors to achieve a site-selective synthesis of nitrogen-doped graphene. All four nitrogen-containing aromatic compounds formed nitrogen-doped graphenes at 500 °C, while nitrogen doping was observed only in the pyridine-derived graphene at 600 °C. The pyridinic-N and pyrrolic-N bonding arrangements were exclusively obtained from quinoline and pyrrole sources, while the pyridine-derived and pyrimidine-derived graphenes contained both pyridinic-N and graphitic-N bonding configuration within the carbon lattice. The nitrogen content and

doped site in the synthesized graphene depended on the source molecule, the origin of which can be interpreted by a bond-reforming model with taking into account the structural stability against heating. On the other hand, nitrogen-doped graphene with nitrogen atoms exclusively at a graphitic site was synthesized from methyl-form by depositing onto a Pt surface at 400 °C. The methyl-form molecules are bound without conjugation by removing the methyl groups at 300 °C, while the conjugation occurred locally at 400 °C leading to N-doped graphene. The ketone-form molecule did not form N-doped graphene at any temperature, while graphene growth occurred at 500 °C due to the production of benzene or its fragment. Thus, the peripheral substituents of the precursor molecules significantly affect the formation of nitrogen-doped graphene. Overall, these results and findings prove the significance of proposed method on the site-selective synthesis of nitrogen-doped graphene. The present result is beneficial for the efficient structural design of a source molecule to achieve the graphene with nitrogen atoms doped at the desired site. Moreover, this study would open a way of controlling the structure of N-doped graphene, leading to the improvement in graphene-based electronic devices or catalysts.

2.6 References

1. K. S. Novoselov, A. K. Geim, S. V Morozov, D. Jiang, Y. Zhang, S. V Dubonos, I. V Grigorieva and A. A. Firsov, *Science*, 2004, **306**, 666–669.

2. K. I. Bolotin, K. J. Sikes, Z. Jiang, M. Klima, G. Fudenberg, J. Hone, P. Kim and H. L. Stormer, *Solid State Commun.*, 2008, **146**, 351–355.

3. A. A. Balandin, S. Ghosh, W. Bao, I. Calizo, D. Teweldebrhan, F. Miao and C. N. Lau, *Nano Lett.*, 2008, **8**, 902–907.

4. M. D. Stoller, S. Park, Z. Yanwu, J. An and R. S. Ruoff, *Nano Lett.*, 2008, **8**, 3498–3502.

5. C. Lee, X. Wei, J. W. Kysar and J. Hone, *Science*, 2008, **321**, 385–388.

6. T. B. Martins, R. H. Miwa, A. J. R. Da Silva and A. Fazzio, *Phys. Rev. Lett.*, 2007, **98**, 3–6.

7. Z.-H. Sheng, H.-L. Gao, W.-J. Bao, F.-B. Wang and X.-H. Xia, *J. Mater. Chem.*, 2012, **22**, 390–395.

8. A. Lherbier, A. R. Botello-Méndez and J. C. Charlier, *Nano Lett.*, 2013, **13**, 1446–1450.

9. L. Qu, Y. Liu, J. B. Baek and L. Dai, *ACS Nano*, 2010, **4**, 1321–1326.

10. L. Zhang and Z. Xia, *J. Phys. Chem. C*, 2011, **115**, 11170–11176.

11. Y. F. Lu, S. T. Lo, J. C. Lin, W. Zhang, J. Y. Lu, F. H. Liu, C. M. Tseng, Y. H. Lee, C. Te Liang and L. J. Li, *ACS Nano*, 2013, **7**, 6522–6532.

12. K. Akada, T. Terasawa, G. Imamura, S. Obata and K. Saiki, *Appl. Phys. Lett.*, 2014, **104**, 131602.

13. T. Schiros, D. Nordlund, L. Pálová, D. Prezzi, L. Zhao, K. S. Kim, U. Wurstbauer, C. Gutiérrez, D. Delongchamp, C. Jaye, D. Fischer, H. Ogasawara, L. G. M. Pettersson, D. R. Reichman, P. Kim, M. S. Hybertsen and A. N. Pasupathy, *Nano Lett.*, 2012, **12**, 4025–4031.

14. X. Kong and Q. Chen, *Phys. Chem. Chem. Phys.*, 2013, **15**, 12982–12987.

15. A. L. M. Reddy, A. Srivastava, S. R. Gowda, H. Gullapalli, M. Dubey and P. M. Ajayan, *ACS Nano*, 2010, **4**, 6337–6342.

16. H. Wang, T. Maiyalagan and X. Wang, *ACS Catal.*, 2012, **2**, 781–794.

17. C. N. R. Rao, K. Gopalakrishnan and A. Govindaraj, *Nano Today*, 2014, **9**, 324–343.

18. S. Sandoval, N. Kumar, A. Sundaresan, C. N. R. Rao, A. Fuertes and G. Tobias, *Chem. - A Eur. J.*, 2014, **20**, 11999–12003.

19. S. Sandoval, N. Kumar, J. Oro-Solé, A. Sundaresan, C. N. R. Rao, A. Fuertes and G. Tobias, *Carbon*, 2015, **96**, 594–602.

20. G. Imamura and K. Saiki, *Chem. Phys. Lett.*, 2013, **587**, 56–60.

21. G. Imamura and K. Saiki, *RSC Adv.*, 2015, **5**, 70522–70526.

22. Y. Wang, Y. Shao, D. W. Matson, J. Li and Y. Lin, *ACS Nano*, 2010, **4**, 1790–1798.

23. Y. Shao, S. Zhang, M. H. Engelhard, G. Li, G. Shao, Y. Wang, J. Liu, I. A. Aksay and Y. Lin, *J. Mater. Chem.*, 2010, **20**, 7491–7496.

24. S. H. Park, J. Chae, M.-H. Cho, J. H. Kim, K.-H. Yoo, S. W. Cho, T. G. Kim and J. W. Kim, *J. Mater. Chem. C*, 2014, **2**, 933–939.

25. T. Matsui, M. Yudasaka, R. Kikuchi, Y. Ohki and S. Yoshimura, *Appl. Phys. Lett.*, 1994, **65**, 2145–2147.

26. C. Zhang, L. Fu, N. Liu, M. Liu, Y. Wang and Z. Liu, *Adv. Mater.*, 2011, **23**, 1020–1024.

27. D. Usachov, O. Vilkov, A. Grüneis, D. Haberer, A. Fedorov, V. K. Adamchuk, A. B. Preobrajenski, P. Dudin, A. Barinov, M. Oehzelt, C. Laubschat and D. V. Vyalikh, *Nano Lett.*, 2011, **11**, 5401–5407.

28. D. Wei, Y. Liu, Y. Wang, H. Zhang, L. Huang and G. Yu, *Nano Lett.*, 2009, **9**, 1752–1758.

29. Z. Luo, S. Lim, Z. Tian, J. Shang, L. Lai, B. MacDonald, C. Fu, Z. Shen, T. Yu and J. Lin, *J. Mater. Chem.*, 2011, **21**, 8038–8044.

30. Z. Jin, J. Yao, C. Kittrell and J. M. Tour, *ACS Nano*, 2011, **5**, 4112–4117.

31. Y. Xue, B. Wu, L. Jiang, Y. Guo, L. Huang, J. Chen, J. Tan, D. Geng, B. Luo, W. Hu, G. Yu and Y. Liu, *J. Am. Chem. Soc.*, 2012, **134**, 11060–11063.

32. T. Terasawa and K. Saiki, *Jpn. J. Appl. Phys.*, 2012, **51**, 055101.

33. J. Li, Z. Ren, Y. Zhou, X. Wu, X. Xu, M. Qi, W. Li, J. Bai and L. Wang, *Carbon*, 2013, **62**, 330–336.

34. J. Zhang, J. Li, Z. Wang, X. Wang, W. Feng, W. Zheng, W. Cao and P. Hu, *Chem. Mater.*, 2014, **26**, 2460–2466.

35. Y. Ito, C. Christodoulou, M. V. Nardi, N. Koch, H. Sachdev and K. Müllen, *ACS Nano*, 2014, **8**, 3337–3346.

36. G. Imamura and K. Saiki, *J. Phys. Chem. C*, 2011, **115**, 10000–10005.

37. G. Imamura, C. W. Chang, Y. Nabae, M. A. Kakimoto, S. Miyata and K. Saiki, *J. Phys. Chem. C*, 2012, **116**, 16305–16310.

38. M. Yamamoto, S. Obata and K. Saiki, *Surf. Interface Anal.*, 2010, **42**, 1637–1641.

39. S. Entani, S. Ikeda, M. Kiguchi, K. Saiki, G. Yoshikawa, I. Nakai, H. Kondoh and T. Ohta, *Appl. Phys. Lett.*, 2006, **88**, 153126.

40. Z. Fang, V. Chellappan, R. D. Webster, L. Ke, T. Zhang, B. Liu and Y.-H. Lai, *J. Mater. Chem.*, 2012, **22**, 15397–15404.

41. J. E. Field and D. Venkataraman, *Chem. Mater.*, 2002, **14**, 962–964.

42. L. Gao, W. Ren, H. Xu, L. Jin, Z. Wang, T. Ma, L.-P. Ma, Z. Zhang, Q. Fu, L.-M. Peng, X. Bao and H.-M. Cheng, *Nat. Commun.*, 2012, **3**, 699.

43. M. Gao, Y. Pan, L. Huang, H. Hu, L. Z. Zhang, H. M. Guo, S. X. Du and H. J. Gao, *Appl. Phys. Lett.*, 2011, **98**, 033101.

44. L. G. Cançado, A. Jorio, E. H. M. Ferreira, F. Stavale, C. A. Achete, R. B. Capaz, M. V. O. Moutinho, A. Lombardo, T. S. Kulmala and A. C. Ferrari, *Nano Lett.*, 2011, **11**, 3190–3196.

45. A. C. Ferrari and J. Robertson, *Phys. Rev. B*, 2000, **61**, 14095–14107.

46. A. C. Ferrari and J. Robertson, *Phys. Rev. B*, 2001, **64**, 075414.

47. A. Eckmann, A. Felten, A. Mishchenko, L. Britnell, R. Krupke, K. S. Novoselov and C. Casiraghi, *Nano Lett.*, 2012, **12**, 3925–3930.

48. C. Y. Su, Y. Xu, W. Zhang, J. Zhao, A. Liu, X. Tang, C. H. Tsai, Y. Huang and L. J. Li, *ACS Nano*, 2010, **4**, 5285–5292.

49. M. Jin, T. H. Kim, S. C. Lim, D. L. Duong, H. J. Shin, Y. W. Jo, H. K. Jeong, J. Chang, S. Xie and Y. H. Lee, *Adv. Funct. Mater.*, 2011, **21**, 3496–3501.

50. S. Wang, X. Wang and S. P. Jiang, *Phys. Chem. Chem. Phys.*, 2011, **13**, 6883–6891.

51. A. E. Axworthy, V. H. Dayan and G. B. Martin, *Fuel*, 1978, **57**, 29–35.

52. Y. Ninomiya, Z. Dong, Y. Suzuki and J. Koketsu, *Fuel*, 2000, **79**, 449–457.

53. J. C. Mackie, M. B. Colket III, P. F. Nelson and M. Esler, *Int. J. Chem. Kinet.*, 1991, **23**, 733–760.

54. G. B. Bacskay, M. Martoprawiro and J. C. Mackie, *Chem. Phys. Lett.*, 1999, **300**, 321–330.

55. A. Doughty and J. C. Mackie, *J. Chem. Soc. Faraday Trans.*, 1994, **90**, 541.

56. A. Lifshitz, C. Tamburu and A. Suslensky, *J. Phys. Chem.*, 1989, **93**, 5802–5808.

57. J. C. Mackie, M. B. Colket III and P. F. Nelson, *J. Phys. Chem.*, 1990, **94**, 4099–4106.

58. N. R. Hore and D. K. Russell, *J. Chem. Soc. Perkin Trans. 2*, 1998, 269–276.

59. A. L. Pinardi, G. Otero-Irurueta, I. Palacio, J. I. Martinez, C. Sanchez-Sanchez, M. Tello, C. Rogero, A. Cossaro, A. Preobrajenski, B. Gómez-Lor, A. Jancarik, I. G. Stará, I. Starý, M. F. Lopez, J. Méndez and J. A. Martin-Gago, *ACS Nano*, 2013, **7**, 3676–3684.

60. Y. Lu and X. Yang, *Carbon*, 2015, **81**, 564–573.

61. M. Martoprawiro, G. B. Bacskay and J. C. Mackie, *J. Phys. Chem.*, 1999, **103**, 3923–3934.

62. A. C. Ferrari and D. M. Basko, *Nat. Nanotechnol.*, 2013, **8**, 235–246.

63. G. W. Cushing, V. Johánek, J. K. Navin and I. Harrison, *J. Phys. Chem. C*, 2015, **119**, 4759–4768.

64. B. Vermang, M. Juel and S. Raaen, *J. Vac. Sci. Technol. A*, 2007, **25**, 1512–1518.

65. G. Franc and A. Gourdon, *Phys. Chem. Chem. Phys.*, 2011, **13**, 14283–14292.

66. J. Cai, P. Ruffieux, R. Jaafar, M. Bieri, T. Braun, S. Blankenburg, M. Muoth, A. P. Seitsonen, M. Saleh, X. Feng, K. Müllen and R. Fasel, *Nature*, 2010, **466**, 470–473.

67. A. L. Pinardi, J. I. Martínez, A. Jančařík, I. G. Stará, I. Starý, M. F. López, J. Méndez and J. Á. Martín-Gago, *Chem. Commun.*, 2014, **50**, 1555–1557.

68. M. Treier, C. A. Pignedoli, T. Laino, R. Rieger, K. Müllen, D. Passerone and R. Fasel, *Nat. Chem.*, 2011, **3**, 61–67.

69. S. Bhaviripudi, X. Jia, M. S. Dresselhaus and J. Kong, *Nano Lett.*, 2010, **10**, 4128–4133.

70. X. Li, C. W. Magnuson, A. Venugopal, J. An, J. W. Suk, B. Han, M. Borysiak, W. Cai, A. Velamakanni, Y. Zhu, L. Fu, E. M. Vogel, E. Voelkl, L. Colombo and R. S. Ruoff, *Nano Lett.*, 2010, **10**, 4328–4334.

71. N. Bonalumi, T. Bürgi and A. Baiker, *J. Am. Chem. Soc.*, 2003, **125**, 13342–13343.

72. Y. T. Kim, J. A. Dumesic and G. W. Huber, *J. Catal.*, 2013, **304**, 72–85.

73. T. T. Pham, L. L. Lobban, D. E. Resasco and R. G. Mallinson, *J. Catal.*, 2009, **266**, 9–14.

74. J. R. Roy, M. A. Laliberté, S. Lavoie, M. Castonguay and P. H. McBreen, *Surf. Sci.*, 2005, **578**, 43–56.

CHAPTER 3

Approaches Towards the Chemical Vapor Deposition Synthesis of Graphitic Carbon Nitride: Critical Role of the Substrate and Annealing Temperature on the Thermal Behavior of Melamine

本章については、５年以内に雑誌等で刊行予定のため、非公開。

CHAPTER 4

Synthesis of Large-Area Atomically Thin Graphitic Carbon Nitride Film via Interfacial Thermal Polymerization of Melamine

本章については、５年以内に雑誌等で刊行予定のため、非公開。

CHAPTER 5

Concluding Remarks

In this thesis, two novel synthesis methods were developed for two different carbon-nitrogen based two-dimensional (2D) crystals: nitrogen-doped graphene (N-Gr) and 2D graphitic carbon nitride (g-C_3N_4). Both methods are bottom-up approaches using only a single species of molecule, which enables to observe the effect of source molecule on the crystal structure. Each of the two crystals was synthesized and characterized by surface science techniques. Moreover, growth mechanisms of these crystals were elucidated by taking full advantage of developed methods. The details of the results presented in the following parts:

Site-selective synthesis of N-Gr from N-containing heterocyclic compounds

In this part, a novel chemical vapor deposition (CVD) method was devised to develop and establish a new approach for the site-selective synthesis of N-Gr. N atoms are mainly doped at three different sites in graphene lattice: graphitic-N, pyridinic-N, and pyrrolic-N site. In the method, six kinds of N-containing heterocyclic compounds were selected and deposited on a heated Pt (111) substrate, respectively, as precursors to achieve a site-selective synthesis of N-Gr. The N-Gr with pyridinic-N and pyrrolic-N bonding arrangement were exclusively obtained from quinoline and pyrrole sources at 500 °C. On the other hand, N-Gr with N atoms exclusively at a graphitic site was synthesized from methyl-form at 400 °C. As a consequence, three doping sites were successfully controlled by using the structure of molecular precursors. The N content and doped site in the synthesized graphene depended on the source molecule, the origin of which can be explained by a bond-reforming model with taking into account the structural stability. The present result is beneficial for the efficient structural design of a source molecule to achieve the graphene with N atoms doped at the desired site. Moreover, this study would

be leading to the improvement in graphene-based electronic devices and catalysts.

Approaches towards the CVD synthesis of g-C_3N_4

In this part, the synthesis of 2D g-C_3N_4 was challenged by using the same CVD method as the former part. In the method, melamine was chosen as a precursor molecule and deposited on Pt (111) and Cu (111) at different temperatures. On Pt (111) substrate, melamine was already decomposed at room temperature, indicates strong catalytic activity of the substrate, which is not preferable for the synthesis of g-C_3N_4. On the other hand, a self-assembled 2D network of melamine was observed for the first time on Cu (111) at 400 °C. However, graphene was formed at 500 °C. The result indicated the substrate with catalytic activity is not suitable for g-C_3N_4 synthesis. Also, the results implied that confined environment is essential for the thermal polymerization to suppress the sublimation and enhance the condensation of melamine molecules. Even though the g-C_3N_4 was not formed, these findings of the critical role of the substrate and annealing temperature on the thermal behavior of melamine are worth for developing the entirely new synthesis method for g-C_3N_4.

Synthesis of large-area atomically thin g-C_3N_4 film via interfacial thermal polymerization of melamine

In this part, a novel synthesis method for 2D g-C_3N_4 using interfacial thermal polymerization of melamine was developed and performed. The development began with the concept of interfacial polymerization and continued throughout the entire design of solid/solid interfacial synthesis of 2D g-C_3N_4. In the method, melamine sandwiched between two solids: a sapphire substrate and Au thin-film were annealed and polymerized to form g-C_3N_4. The as-prepared films on sapphire substrates were mainly characterized by XPS and AFM. From XPS analysis, the chemical structure of the as-synthesized film well agreed with the g-C_3N_4. The AFM measurement revealed that the surface of the film was uniformly flat, and the film had a thickness of ~ 1 nm. Therefore, the formation of 2D g-C_3N_4 was confirmed. Further, to elucidate the growth mechanism of the devised method, synthesis conditions were varied to observe the influence of synthetic parameters.

It was revealed that pressurization plays two important roles during the synthesis process of 2D g-C_3N_4.

In this thesis, novel synthesis methods for 2D crystals were developed and demonstrated. As mentioned, certain objectives were achieved in this study. However, there remains huge gap between these activities and industrial application or production of 2D materials. A key requirement for application of 2D materials is the development of synthesis method. In this regard, more efforts should be devoted to advancing this field. Also, there are several further analyses needs to be considered in this study. Especially, atomic scale imaging of 2D crystal structure using scanning tunneling microscopy (STM) or transmission electron microscopy (TEM) should be considered. This analysis enables more precise structural evaluation of 2D crystal. The transfer method is also required to transfer 2D crystals from growth substrate to conductive surface or TEM grid. These works contribute to developing methods optimized for 2D material synthesis and are beneficial for the future application of 2D materials.

ACKNOWLEDGEMENT

I would like to extend my sincerest gratitude and appreciation to those who helped me accomplish this study.

I would first like to express a tremendous appreciation to my supervising professor, Prof. Koichiro Saiki, for supporting me patiently, continuous discussions and suggestions. I would also like to express my appreciation to Prof. Takehiko Sasaki for the active discussion and valuable inputs made through the weekly seminar. I would like to sincerely thank Prof. Hideki Yorimitsu in Kyoto University, for supplying organic molecules of my experiment and giving me a lot of insightful and constructive suggestions.

I would also like to express my sincere appreciation to Dr. Seiji Obata and Dr. Gaku Imamura. I truly appreciate Dr. Obata for invaluable support and advice at every discussion and keep me encouraged and support me in experiments and daily life since I joined this laboratory. Special thanks are also extended to Dr. Imamura (NIMS) for giving me constructive criticisms, and valuable comments and continued support led me to the doctoral course.

I also want to express my thanks and appreciation to Dr. Terasawa, Dr. Kotsuki, and Dr. Akada, who supported me in daily research life. The only regret I have is that I cannot go for a meal together because of my poverty.

My appreciation extended to the other members of Saiki Laboratory. It was my precious time when chatted each other for various topics every day.

Finally, I would like to extend my appreciation to my family for their support and encourage for five years.

APPENDIX

A. Estimation of interfacial pressure

本付録は、５年以内に雑誌等で刊行予定の、４章の内容に含まれるため、非公開。